Astron. Astrophys. 329, 291–314 (1998)

ASTRONOMY
AND
ASTROPHYSICS

# CHIANTI: an atomic database for emission lines

## II. Comparison with the SERTS-89 active region spectrum

**P.R. Young**[1], **E. Landi**[2], **and R.J. Thomas**[3]

[1] Department of Applied Mathematics and Theoretical Physics, University of Cambridge, UK
[2] Department of Astronomy and Space Science, University of Florence, Italy
[3] Laboratory for Astronomy and Solar Physics, NASA-Goddard Space Flight Center, Greenbelt MD 20771, USA

Received 24 June 1997 / Accepted 4 August 1997

**Abstract.** The CHIANTI database was described by Dere et al. (1997, hereafter Paper I) and the present paper applies the atomic data to the study of extreme ultra-violet emission lines found in the SERTS-89 active region spectrum published by Thomas & Neupert (1994). Firstly, the emission line ratios that are insensitive to density and temperature are used to check both the quality of the atomic data and the calibration of the instrument. Secondly, we use, where possible, ratios that are sensitive to density to estimate the electron density from different ions.

In general we find excellent agreement between theory and observation, providing confidence in both the atomic data in the CHIANTI database and the quality of the SERTS-89 spectrum. Where inconsistencies between theory and observation exist we try to explain them in terms of either inaccuracies in the atomic data or blending of the lines. One consistent discrepancy was that all observed lines that we analysed in the 430–450 Å region were uniformly a factor of 1.5–2.0 weaker than predicted, suggesting that the SERTS-89 calibration may need adjustment in this spectral interval. Serious problems were also found in some of the theoretical predictions for a few ions, especially Fe XIV.

**Key words:** atomic data – astronomical data bases: miscellaneous – Sun: UV radiation

### 1. Introduction

The CHIANTI database, described in Paper I, aims to provide solar and stellar researchers with access to the best available atomic data from which the emission lines of all the major atomic species can be studied using IDL routines. An important part of the CHIANTI project is to check the accuracy of the atomic data by comparing the observed intensities of emission lines recorded by various rocket and satellite missions with the intensities predicted by CHIANTI. The first of such comparisons is presented here with regard to the recently published active region spectrum of Thomas & Neupert (1994). Comparisons with Extreme Ultra-Violet Explorer (EUVE) and Solar and Heliospheric Observatory (SOHO) data will follow.

The details of the SERTS-89 spectrum and the method of analysis are presented below, followed by the detailed comparison of each ion with theory.

*Send offprint requests to*: P.R. Young

### 2. The SERTS-89 spectrum

The Solar EUV Rocket Telescope and Spectrograph (SERTS) has been flown on several occasions, returning the highest quality imaged extreme ultra-violet (EUV) spectra yet obtained of the Sun. A spectrum of an active region obtained in the 1989 flight was published by Thomas & Neupert (1994) and we will henceforward refer to this flight as SERTS-89.

The SERTS-89 instrument covered the 235–450 Å wavelength region in first order and 170–225 Å in second order, with sensitivity greatest above 300 Å as witnessed by Fig. 2 of Thomas & Neupert. The spectral resolution of nearly 10,000 is the highest yet achieved for this wavelength region, with line positions measured to a precision of 5 mÅ or better in most cases.

The published spectrum represents an average over an area of around $7'' \times 276''$ across a solar active region. Subsequent re-evaluation of the absolute calibration scale for SERTS-89 indicates that all intensities reported in the catalogue should be increased by a factor of 1.24. However, to simplify comparison and because we are interested here only in relative values, we will continue to use the original intensity scale in the present work.

### 3. Method of analysis

The quality of the SERTS-89 spectrum has meant that for a lot of the transition region and coronal ions we have several lines

identified for a single species, thus allowing a detailed comparison of theory with observations. One such attempt at a detailed comparison is that of Brickhouse et al. (1995) who studied only the iron ions and used every observed line to compare with theory. Fig. 1 of their work shows a comparison assuming an electron density of $10^{10}$ cm$^{-3}$ for all the ions, while in Fig. 6 of their work they use density diagnostic pairs for the ions to estimate average electron densities. In each case we see a large spread in derived values.

In this work, we argue that while every line in the spectrum for a given ion should be used they should not be used in an average sense but instead be used firstly as a check on both the atomic data and the instrument calibration and secondly as a means of determining plasma parameters such as density and emission measure.[1] The first step in this process is to look for *density insensitive* line ratios. These come in two forms and we will differentiate *branching ratios* from ratios whose insensitivity stems from, e.g., the lines being principally excited from the same lower level (these we will refer to as simply density insensitive ratios). The reason for this differentiation is that the atomic data required to predict branching ratios are simply the transition probabilities which can generally be calculated to accuracies of $< 10\%$. For density insensitive ratios we need to have estimates of the electron excitation rates which are rather more difficult to calculate and so less accurate (typically 30% or less).

The use of ratios insensitive to the electron density as a means of determining the calibration of solar EUV instrumentation has been discussed by Neupert & Kastner (1983) where references to earlier work can be found. The quality of atomic data for many ions has improved substantially since this work, so allowing far more density insensitive ratios to be identified, while the CHIANTI database ensures that all of this data is easily accessible.

The advantage of density insensitive ratios over branching ratios lies in the fact that they can span large regions in wavelength, whereas lines related by branching ratios tend to lie close to one another (usually within 20 Å). As an example, one can see the five Fe XIV branching ratios in Table 18 which each involve lines within 23 Å of each other, whereas the density insensitive ratios presented in Table 19 involve lines separated by up to 110 Å. A disadvantage is that the density insensitive ratios are often not strictly density insensitive and may also show some temperature sensitivity.

In choosing *density sensitive* ratios to study, we try to avoid any redundancy in the lines. For example, for lines $a$, $b$ and $c$, say; if $a$ and $b$ are related by a branching ratio and agree well with theory, and if $a$ and $c$ are density sensitive and yield a density of $10^{10}$ cm$^{-3}$, say, then we can immediately guess that the $b/c$ ratio will also yield a density of around this value. The most extreme example of this removal of redundancy can be seen in Fe XIII where, starting from the observed 23 lines, we reduce the number of density diagnostic ratios down to 4 which are shown in Table 20. The consistency between these ratios is reasonable and contrasts strongly with Fig. 6 of Brickhouse et al. (1995) where they show densities spanning 3 orders of magnitude. The reason for this difference is that our method eliminates weak lines or lines inconsistent with theory at the initial density-insensitive ratio stage. Thus, the lines we use to predict densities are typically strong lines that are known to be consistent with theory in terms of insensitive ratios.

We choose to go through the different ions by iso-electronic sequence, each of which commands a section to itself, and discuss each ion within the sequence separately. The exceptions to this are the iron and nickel ions which are rather more complex and deserving of a separate section. Each section has three tables displaying branching ratios, density insensitive ratios and density sensitive ratios. An explanation of the symbols used in these tables is given in Sect. 5.

## 4. Use of the CHIANTI database

The CHIANTI database contains both atomic data and a set of routines which enable the line intensities to be calculated and analysed. For this work, two of the authors (E. Landi and P. Young) have used the atomic data but not the CHIANTI analysis routines, instead they have interfaced their own existing routines to the atomic data. In particular, E. Landi has used the new L-function method of analysis (Landi & Landini 1997) to check the results obtained with the intensity ratio method for several ions. P. Young has used routines which allow the input of proton collision rates to the level balance program – a feature not accounted for in the original version (1.0) of CHIANTI. Thus, for this work, we have proton rates included for the following ions: Ne VI, Mg VIII, Si X, S XII, Fe X, Fe XIII and Fe XIV.[2] For these ions one may find differences between values quoted here and those derived using the CHIANTI analysis routines, however such differences are likely to be small as proton rates do not contribute significantly to the level balance of these ions.

## 5. Guide to the tables

The wavelengths of all the lines in the tables are those of Thomas & Neupert (1994) rounded to two decimal places, except for those lines not in the catalogue. Some of the lines will have a superscript that indicates one of the following:

[1] This method is essentially that of Young & Mason (1996) who applied it to the Fe XIV lines seen in the SERTS-89 spectrum.

[2] Proton rates for the boron-like ions are taken from Foster et al. (1997), Fe X from Bely & Faucher (1970), Fe XIII from Landman (1975), and Fe XIV from Heil et al. (1983).

b Blend with a line from another element. The intensity used includes the blended component(s).
s Blend of two or more lines from the same element.
n A line not identified by Thomas & Neupert, but relevant to the discussion of the ion.
i A line not identified by Thomas & Neupert, but suggested as either a new identification or as a component to a line in the spectrum.
c Blended line, but one in which the individual contributions of each component can be estimated and used in the specified ratio.

For the ratios displayed, the following symbols are used:

◁ An observed ratio that does not agree with the theoretical value within the error bars of the data.
◁◁ As above, but discrepancy is a factor of two or greater.
T An 'insensitive' ratio whose variation is due principally to temperature effects, instead of the usual density dependence.

Some other symbols used throughout the text are:

$T_{\rm max}$ The temperature of maximum ionization of the ion, from Arnaud & Raymond (1992) for the iron ions, and from Arnaud & Rothenflug (1985) for all other ions.
$Z$ The atomic number of the element.
$N_{\rm e}$ The electron number density in $\rm cm^{-3}$.

The values of the theoretically 'density insensitive' ratios are obtained by simply taking the mean of that ratio over a number of different densities, e.g., $10^8 - 10^{12}\,\rm cm^{-3}$, while the error bars come from the standard deviation of this set of numbers. If temperature sensitivity is strongest then the same procedure is applied over the temperature range $\log T_{\rm max} - 0.15$ to $\log T_{\rm max} + 0.15$.

In some cases, CHIANTI predicts lines not found in the SERTS-89 catalogue. If such lines are potentially useful as a density diagnostic, then an upper limit based on the $3\sigma$ sensitivity level (see Table 2 of Thomas & Neupert) is used to provide a constraint on the predicted density.

## 6. Hydrogen iso-electronic sequence

### *6.1. He II*

Checking the consistency of the four He II lines seen in the SERTS-89 spectrum is difficult as the line ratios are very sensitive to temperature. Furthermore, the 256.32/303.78 ratio is also strongly density sensitive, and 256.32 Å is a known blend with Si X. However, we can estimate the contribution of Si X to the blend with some confidence (see Sect. 9.4). Even taking that into account, the observed He II 256.32/303.78 ratio of $0.023 \pm 0.006$ lies close to the low density limit (0.028 at a density of $10^8\,\rm cm^{-3}$) for a temperature of $\log T = 4.7$ (the $\log T_{\rm max}$ of He II) – a lower temperature of around $\log T = 4.5$ is required to give higher, more realistic densities.

**Table 1.** Insensitive ratios for He II.

| Ion | Ratio | Theory | SERTS-89 |
|---|---|---|---|
| He II | 243.03 / 303.78 | $0.0066 \pm 0.0003$ | $0.0077 \pm 0.0023$ |
| | 237.35 / 303.78 | $0.0026 \pm 0.0002$ | $0.0050 \pm 0.0018$ ◁ |

**Table 2.** Insensitive ratios for Li-like ions.

| Ion | Ratio | Theory | SERTS-89 |
|---|---|---|---|
| C IV | 384.03 / 384.17$^{\rm s}$ | 0.50 | $0.91 \pm 0.42$ |
| | 419.72 / 384.17$^{\rm s}$ | $0.91 \pm 0.23^{\rm T}$ | $1.31 \pm 0.43$ |
| | 312.43$^{\rm s}$/ 384.17$^{\rm s}$ | $0.93 \pm 0.11^{\rm T}$ | $1.49 \pm 0.85$ |
| S XIV | 445.66 / 417.64 | 0.47 | $0.36 \pm 0.09$ ◁ |
| Ar XVI | 389.08$^{\rm b}$/ 353.96 | 0.46 | $1.7 \pm 0.8$ |
| Ca XVIII | 344.77 / 302.17 | 0.45 | $0.54 \pm 0.28$ |

The 243.03/303.78 and 237.35/303.78 ratios are insensitive to density and we give comparisons with theory in Table 1. As the temperature sensitivity is large for He II, we only give the theoretical values of the ratios at the $T_{\rm max}$ of the ion. The agreement of the 243.03/303.78 is excellent, but that of 237.35/303.78 less good, perhaps because the 237.35 Å line lies close to the low wavelength end of the spectrometer.

## 7. Lithium iso-electronic sequence

The emission spectrum of Lithium-like ions is dominated by the $2s\ ^2S_{1/2} - 2p\ ^2P_{1/2,3/2}$ transitions, the most well-known of which are the C IV 1548 Å and 1550 Å lines. In the SERTS-89 waveband, we find some of the weaker n=2 to n=3 transitions of C IV, together with the aforementioned doublet of the sulphur, argon and calcium ions.

### *7.1. C IV*

Four lines of C IV are identified in the spectrum, all of which are density insensitive relative to each other. There are two lines predicted by CHIANTI at 419.71 Å and 419.52 Å, and related to each other by a branching ratio (the 419.52 Å line is a decay to the $^2P_{1/2}$ level). Only the former transition is identified, and is found at 419.72 Å with intensity 12.4 erg $\rm cm^{-2}\,s^{-1}\,sr^{-1}$. From the branching ratio we can estimate an intensity for the 419.52 Å line of 6 erg $\rm cm^{-2}\,s^{-1}\,sr^{-1}$, making it potentially observable, yet no line is found in the spectrum at this wavelength.

The line at 384.17 Å is actually a blend of the reported $^2P_{3/2} - {}^2D_{5/2}$ transition with the $^2P_{3/2} - {}^2D_{3/2}$ transition, although the latter only contributes around 10% of the line intensity. We take three density insensitive ratios relative to this line and display the comparisons with theory in Table 2. Agreement within the error bars is found for all three. Note that the error bars on the

theoretical data are due to temperature sensitivity of the ratios. Since the error bars on the observed data are larger than this temperature sensitivity, we can not use the lines to estimate a temperature for the plasma.

Keenan et al. (1993a) compared the C IV lines observed by SERTS-89 with theory and found the same results as those given here.

### *7.2. S XIV, Ar XVI, Ca XVIII*

Only the $^2$S – $^2$P lines mentioned previously are seen for these ions, and they show no relative temperature or density sensitivity. Comparisons with observations are presented in Table 2.

Despite the strength of the two S XIV lines, the observed ratio disagrees marginally with theory. This may reflect an inaccuracy in the calibration of the instrument at the longest wavelengths, as is discussed further in Sect. 15.1.

The Ca XVIII ratio is found to be in agreement with the observations, while from the Ar XVI ratio we can estimate a Ar XVI contribution of 3.5 erg cm$^{-2}$ s$^{-1}$ sr$^{-1}$ to the 389.08 Å line's total of 12.8 erg cm$^{-2}$ s$^{-1}$ sr$^{-1}$. The other component is due to Fe XVII and is discussed in Sect. 13.9.

### *7.3. Summary*

Very few lithium-like ion lines are seen in the SERTS-89 waveband and no density diagnostics are available. The observed lines can instead be used as a check on the atomic data adopted by the CHIANTI database. The features we have found are as follows:

- Agreement with theory is reasonable.
- The S XIV 445.66/417.64 ratio shows a mild discrepancy which may be due to calibration errors.

## 8. Beryllium iso-electronic sequence

The EUV spectra of the Beryllium-like ions is dominated by the 2s$^2$ $^1$S$_0$ – 2s2p $^1$P$_1$ transition which can be seen in the SERTS-89 observations from consecutive elements sodium through to sulphur. Of these elements, it is only for Mg IX and Si XI that we find lines other than this, namely the 2s$^2$ $^3$P – 2s2p $^3$P transitions. For O V, weak 2p – 3s lines are identified.

### *8.1. O V*

The two O V lines in the Thomas & Neupert catalogue are both very weak identifications: 215.29 Å is a weak feature seen in the wing of first order Mg VIII 430.45 Å, while the 248.46 Å occurs close to the low wavelength end of the spectrometer bandpass, where the sensitivity is lowest.

The 215.29 Å line seems unlikely to be a O V feature as we would then have expected the O V 220.35 Å line to have appeared in second order at around 440.70 Å, as it has an intensity at least as strong as the 215.29 Å line. However, nothing is seen there despite it being a fairly "blank" part of the spectrum.

**Table 3.** Branching ratios for the Beryllium-like ions.

| Ion | Ratio | Theory | SERTS-89 |
|---|---|---|---|
| Mg IX | 439.17 / 443.96 | 0.35 | $0.48 \pm 0.15$ |
| | 443.37 / 441.22 | 0.74 | $0.73 \pm 0.36$ |
| | 448.28 / 441.22 | 1.17 | $0.61 \pm 0.30$ ◁ |
| Si XI | 358.65$^{i}$/ 365.43 | 0.36 | – |
| | 364.50$^{i}$/ 361.41 | 0.72 | – |
| | 371.50 / 361.41 | 1.12 | $0.61 \pm 0.19$ ◁ |

We show the 248.46/220.35 ratio in Table 4 to give an indication of the expected intensity of the 220.35 Å line. The error bars on the theoretical ratio are due principally to temperature sensitivity which is quite marked for these two lines despite their closeness in wavelength.

### *8.2. Mg IX*

A comparison of SERTS-89 Mg IX intensities with theory was provided by Keenan et al. (1994a). We note that they used older RMATRX calculations (Keenan 1988, Berrington 1985) whereas in the CHIANTI database we use the more recent Distorted Wave calculations of Zhang & Sampson (1992).

For the six identified lines we find three branching ratios which are given in Table 3. The 448.28/441.22 ratio is discrepant by almost a factor of two with the 448.28 Å line being weaker than expected. Keenan et al. find a similar result, and suggest that this is an instrumental effect due to the 448.28 Å line falling close to the high wavelength end of the SERTS-89 bandpass.

There are two regions of density sensitivity in Mg IX: first the 2s2p $^3$P$_0$ and $^3$P$_2$ levels gain significant populations (relative to the ground $^1$S$_0$ level) at $\simeq 10^9$ cm$^{-3}$ and then the 2s2p $^3$P$_1$ level gains a significant population for densities greater than $10^{12}$ cm$^{-3}$. Between $10^9$ cm$^{-3}$ and $10^{12}$ cm$^{-3}$ the Mg IX ratios are density insensitive and the ratios reported in Table 4 apply *only* to this density regime for these lines.

The 441.22 Å and 448.28 Å lines give density insensitive ratios relative to 443.96 Å and we give both ratios in Table 4. They potentially allow a determination of which of the 441.22 Å and 448.28 Å lines is in error, but both ratios are consistent within the error bars on the data.

The low value of the observed 443.96/368.06 ratio means that it falls within the $< 10^9$ cm$^{-3}$ density sensitive regime and so we give the density that it indicates in Table 5. Similarly, although the 441.22/443.96 insensitive ratio agrees with theory within the error bars on the data, the fact that the observed value lies above the theoretical value means that the same ratio can be used to derive a density. In both cases the density is somewhat low and not consistent with other ions formed at the same temperature.

In their analysis, Keenan et al. (1994a) assume a density of $10^{10}$ cm$^{-3}$ and compare the observed line intensities with theory, finding good agreement apart from with the aforementioned

**Table 4.** Insensitive ratios for the Be-like ions.

| Ion | Ratio | Theory | SERTS-89 |
|---|---|---|---|
| O V | 248.46 / 220.35[n] | $1.23 \pm 0.26$[T] | – |
| Mg IX | 443.96 / 368.06 | $0.030 \pm 0.004$[T] | $0.018 \pm 0.004$ ◁ |
| | 441.22 / 443.96 | 0.28 | $0.39 \pm 0.16$ |
| | 448.28 / 443.96 | 0.32 | $0.24 \pm 0.09$ |
| Si XI | 361.41 / 365.43 | $0.30 \pm 0.03$ | $0.60 \pm 0.14$ ◁ |
| | 371.50 / 365.43 | $0.34 \pm 0.03$ | $0.36 \pm 0.11$ |

**Table 5.** Density sensitive line ratios for the Be-like ions.

| Ion | Ratio | SERTS-89 | Log $N_e$ |
|---|---|---|---|
| Mg IX | 443.96 / 368.06 | $0.018 \pm 0.004$ | $8.4^{+0.2}_{-0.2}$ |
| | 441.22 / 443.96 | $0.39 \pm 0.16$ | $7.8^{+hi}_{-0.4}$ |
| Si XI | 365.43 / 303.32 | $0.014 \pm 0.003$ | $9.2^{+0.2}_{-0.2}$ |

448.28 Å line. We note that although their theoretical value for the 443.96/368.06 ratio is smaller than ours (0.026 compared to 0.030), it remains outside the error bars of the observed data. The reason for their smaller predicted ratio stems mainly from their larger value of the 368.06 Å thermally-averaged collision strength (1.59 compared to our 1.20).

The disagreement of the Mg IX 443.96/368.06 ratio with theory may reflect an error in the intensity calibration curve of SERTS-89, as discussed later in Sect. 15.1.

### *8.3. Si XI*

The excellent spectral resolution of the SERTS instrument ensures that the Si XI 303.32 Å line is well separated from the far stronger He II line at 303.78 Å, which has not been possible with previous imaging spectrometers. Only three of the five $^3$P – $^3$P transitions are identified in SERTS-89, and there is relative density sensitivity between the $^3$P lines and the strong 303.32 Å line in the density range $10^7$–$10^{10}$ cm$^{-3}$. Care has to be taken below densities of around $10^8$ cm$^{-3}$ as photo-excitation by a background radiation field can play an important role in depopulating the 2s2p $^3$P$_0$ level, significantly affecting the level balance of the ion. This process is not accounted for in the current version (1.0) of CHIANTI.

The two $^3$P – $^3$P transitions not identified by Thomas & Neupert are predicted by CHIANTI to be at 358.65 Å and 364.50 Å and are both strong enough to have been observed, as witnessed by the branching ratios presented in Table 3. Both lines are however blended with other stronger lines and so we use the branching ratios to predict Si XI contributions to each blend.

The CHIANTI 358.65 Å line is blended with the reported Fe XI 358.67 Å line. As discussed in Sect. 13.3, the latter line at 73 erg cm$^{-2}$ s$^{-1}$ sr$^{-1}$ is a factor 3 too strong, consistent with the presence of a blend; however, the Si XI component only provides around 14 erg cm$^{-2}$ s$^{-1}$ sr$^{-1}$. Other components are suggested to be from Ne IV and Fe XIV.

The line expected at 364.50 Å is blended with the stronger Fe XII 364.47 Å line. From the branching ratios we can estimate a Si XI contribution of 17 erg cm$^{-2}$ s$^{-1}$ sr$^{-1}$ to the observed total intensity of 233 erg cm$^{-2}$ s$^{-1}$ sr$^{-1}$ for this feature.

The observed 371.50/361.41 ratio is not in agreement with theory and although there is an Fe X line predicted by CHIANTI at 361.40 Å it is not strong enough to account for the discrepancy. Of interest is the fact that observations for the corresponding transitions in Mg IX (448.28/441.22) were also inconsistent with the theoretical branching ratio and by a similar amount, the 371.50 Å and 448.28 Å lines being both around a factor of two too low. This suggests that there may be a problem with the transition probabilities for these two transitions.

As the 2p$^2$ $^3$P$_0$ and $^3$P$_2$ levels do not come into Boltzmann equilibrium with the ground level until densities $> 10^{10}$ cm$^{-3}$, we can use the 365.43/303.32 ratio to estimate a density (given in Table 5) that is consistent with other elements formed at the same temperature.

Above $10^9$ cm$^{-3}$, the 361.41/365.43 and 371.50/365.43 ratios become density insensitive with values shown in Table 4. Interestingly, it is the 371.50/365.43 ratio rather than the 361.41/365.43 ratio which agrees better with theory, which suggests that the 361.41 Å line may be blended.

### *8.4. Summary*

The relative density sensitivity of the beryllium-like ion lines tends to be small over typical coronal densities of $10^{8.5}$ – $10^{11}$ cm$^{-3}$ and so the line ratios are not useful as density diagnostics, apart from the Si XI 365.43/303.32 ratio. The main features of the Be-like lines are as follows.

- The $^1$S – $^1$P transition does not show agreement with the $^3$P – $^3$P transitions for Mg IX unless a small density of around $10^{8.4}$ cm$^{-3}$ is assumed. The same ratios for Si XI can be used to give a density consistent with other ions formed at similar temperature, and so we suggest that it is only for Mg IX that there is a real problem. One possibility is that the SERTS-89 calibration may require some adjustment above 430 Å.
- Observed ratios of ($^3$P$_2$ – $^3$P$_1$)/($^3$P$_0$ – $^3$P$_1$) lines for both Mg IX and Si XI are around a factor of two too low compared with predicted branching ratios, suggesting that presently accepted transition probabilities for both ions are incorrect. On the other hand, such a large error is difficult to explain in terms of atomic physics, and so an alternative suggestion is that the Mg IX 448.28 Å line is under-estimated due to optical vignetting since it is very close to the high wavelength end of the SERTS-89 bandpass, whereas the Si XI 361.41 Å line may be affected by blends.

## 9. Boron iso-electronic sequence

The dominant EUV transitions of the boron-like ions arise from 2s$^2$–2s2p doublet-doublet transitions. There are nine such transitions corresponding, in ascending wavelength order, to $^2$P–

**Table 6.** Branching ratios for the B-like ions.

| Ion | Ratio | Theory | SERTS-89 |
|---|---|---|---|
| Ne VI | 399.84 / 401.94 | 0.20 | $0.18 \pm 0.04$ |
| | 403.30[b]/ 401.14 | 0.58 | $1.53 \pm 0.28$ |
| | 433.16 / 435.63 | 0.60 | $0.77 \pm 0.35$ |
| Mg VIII | 311.78[b]/ 315.02 | 0.19 | $0.31 \pm 0.07$ |
| | 317.01 / 313.74 | 0.71 | $0.72 \pm 0.20$ |
| | 335.25[n]/ 339.00 | 0.75 | – |
| Al IX | 280.15[n]/ 284.04[n] | 0.19 | – |
| | 286.38[n]/ 282.43 | 0.79 | – |
| | 305.09 / 300.56 | 1.09 | $0.56 \pm 0.17$ ◁ |
| Si X | 253.81 / 258.37 | 0.19 | $0.55 \pm 0.17$ ◁◁ |
| | 256.32[b]/ 261.05 | 1.12 | $11.3 \pm 0.17$ |
| | 277.27 / 271.99 | 0.82 | $0.87 \pm 0.25$ |
| S XII | 299.79[n]/ 288.40 | 0.11 | – |

**Table 7.** Insensitive ratios for the B-like ions.

| Ion | Ratio | Theory | SERTS-89 |
|---|---|---|---|
| Ne VI | 401.14 / 401.94 | 0.38 | $0.35 \pm 0.06$ |
| | 435.63 / 401.94 | $0.28 \pm 0.01$[T] | $0.12 \pm 0.03$ ◁ |
| Mg VIII | 339.00 / 315.02 | 0.23 | $0.21 \pm 0.04$ |
| | 430.45 / 313.74 | $0.95 \pm 0.08$[T] | $0.50 \pm 0.10$ ◁ |
| | 436.73[s]/ 315.02 | $0.61 \pm 0.06$[T] | $0.27 \pm 0.05$ ◁ |
| Al IX | 305.09 / 284.04[n] | $0.21 \pm 0.01$ | – |
| | 385.02 / 282.43 | $1.02 \pm 0.08$[T] | $0.25 \pm 0.13$ ◁◁ |
| | 305.09 / [385,392]† | $0.22 \pm 0.02$[T] | $0.78 \pm 0.37$ ◁ |
| Si X | 271.99 / 261.05 | 0.76 | $0.94 \pm 0.25$ |
| | 347.41 / 261.05 | $1.39 \pm 0.14$[T] | $1.50 \pm 0.45$ |
| | 356.03[s]/ 258.37 | $0.51 \pm 0.06$[T] | $0.58 \pm 0.11$ |

†A sum of the lines at 385.02 Å and 392.41 Å.

$^2$P (4 lines), $^2$P–$^2$S (2 lines), and $^2$P–$^2$D (3 lines) transitions. For ions with $Z > 11$ the ground $^2$P levels do not come into Boltzmann equilibrium until the electron density is at transition region/coronal densities and so yield useful density diagnostics. For $Z < 11$ ions density sensitivity comes from the $2s2p^3$ $^4$P levels coming into Boltzmann equilibrium with the ground levels, but this is not relevant for the SERTS-89 lines.

### *9.1. Ne VI*

The $^2$P–$^2$D transitions lie outside the SERTS-89 bandpass at around 558–563 Å, while the remaining six transitions lie at around 400 Å and 430 Å. For typical transition region densities of $10^8 - 10^{12}$ cm$^{-3}$ each of the six Ne VI observed lines are density insensitive relative to each other. There are three branching ratios and their values are in agreement with observation and reported in Table 6. The line at 403.30 Å is blended with a Mg VI line and the branching ratio 403.30/401.14 allows the Ne VI contribution to be estimated at around 17 erg cm$^{-2}$ s$^{-1}$ sr$^{-1}$ out of the total blended intensity of 45.6 erg cm$^{-2}$ s$^{-1}$ sr$^{-1}$.

There is a discrepancy between the theoretical intensity ratios involving the two lines at 433.16 Å and 435.63 Å and the other four observed transitions (see Table 7), with the former being around a factor of two too low. This is discussed later with regard to the calibration of the spectrometer.

### *9.2. Mg VIII*

All of the nine transitions occur in the SERTS-89 wavelength range, although the line expected at 335.25 Å is hopelessly masked by the far stronger Fe XVI 335.40 Å line in the active region spectrum. From the branching ratio 335.25/339.00 (see Table 6) we can estimate that the expected intensity of the Mg VIII line is around 40 erg cm$^{-2}$ s$^{-1}$ sr$^{-1}$, as compared to the observed Fe XVI intensity of 10400 erg cm$^{-2}$ s$^{-1}$ sr$^{-1}$. However, Mg VIII may well be important and can even dominate the emission at this wavelength for cooler solar features, such as quiet Sun or coronal holes.

The 311.78 Å line is blended with a Ni XV line, and we use the 311.78/315.02 branching ratio to evaluate the Mg VIII contribution as around 48 erg cm$^{-2}$ s$^{-1}$ sr$^{-1}$ out of the observed total of 79 erg cm$^{-2}$ s$^{-1}$ sr$^{-1}$. The remaining branching ratio pair are well observed and are consistent with theory.

A weak transition is expected at 436.67 Å but is blended with the stronger 436.73 Å line, and only the latter is reported in the Thomas & Neupert catalogue. The contribution of the weaker line is expected to be 1/10 of the total intensity. Both lines have been considered for the intensity ratios here.

For the three density insensitive ratios given in Table 7 we see clearly that the lines at 430.45 Å and 436.73 Å are around a factor two lower than theory predicts. We feel that this may indicate a calibration problem, as discussed later in Sect. 15.1.

The ground $^2$P levels come into Boltzmann equilibrium for densities around $10^9$ cm$^{-3}$ and thus it is possible to use the Mg VIII lines to estimate the plasma density. Two ratios are suggested in Table 8, although both only give lower limits to the density. They are more useful for quiet Sun or coronal hole observations where the density is lower.

Bhatia & Thomas (1997) have recently reported new atomic data calculations for Mg VIII, as well as comparisons with SERTS-89 observations. Their conclusions are very similar to those presented here.

### *9.3. Al IX*

The nine Al IX transitions all fall within the bandpass of the SERTS-89 spectrometer but only five are reported in the Thomas & Neupert catalogue. One surprise is the absence of the multiplet $2s^22p\ ^2P - 2s2p^2\ ^2P$ with the exception of the 282.43 Å line. The strongest line of this multiplet (and of the entire Al IX spectrum) is expected to be observed at 284.04 Å, but lies close to the very strong Fe XV 284.16 Å line and so can not be reliably fitted. Branching ratios for the $^2$P – $^2$P multiplet are given

in Table 6, while we give the density insensitive 305.09/284.04 ratio in Table 7 to give an indication of the expected intensity of the 284.04 Å line. The 300.56/305.09 branching ratio is not consistent with observations, and we suggest that the 300.56 Å line may be blended.

From Table 7 it is clear that the two lines observed at 385.02 Å and 392.41 Å are considerably weaker than expected as estimated from the 282.43 Å and 305.09 Å lines. We note that the same behavior is seen in the corresponding transitions of Mg VIII, although in that case the discrepancies were thought to indicate inaccuracies in the intensity calibration curve.

Although both the 305.09/282.43 and 300.56/282.43 ratios are density sensitive below around $10^{9.5}$ cm$^{-3}$, the error bars on the data are actually greater than the variation of the ratios with density. Despite this, we list both ratios in Table 8 and note that better agreement is found for the 305.09/282.43 ratio, strengthening the suggestion above that the 300.56 Å line is blended.

The 392.41/385.02 ratio has been recognised previously as a useful density diagnostic below around $10^{9.5}$ cm$^{-3}$ (see, e.g., Keenan et al. 1994b), and with the SERTS-89 data we can derive a lower limit to the density, as shown in Table 8.

### *9.4. Si X*

Again all nine boron-like transitions are found in the SERTS-89 spectral range, and all of them have been reported in the Thomas & Neupert catalogue. In addition there is a line identified at 292.25 Å as Si X, but we dismiss this identification as the Si X line predicted by CHIANTI at this wavelength is expected to be around two orders of magnitude weaker than the observed line. The line at 256.32 Å is blended with a stronger He II line; the Si X contribution can be estimated from the branching ratio presented in Table 6 as around 157 erg cm$^{-2}$ s$^{-1}$ sr$^{-1}$ out of the observed total of 1580 erg cm$^{-2}$ s$^{-1}$ sr$^{-1}$.

The 253.81/258.37 branching ratio shows a strong discrepancy with observations (Table 6), but we note that in the Malinovsky & Heroux (1973) quiet Sun spectrum this ratio was 0.19, suggesting that the SERTS-89 value may be in error. The remaining density insensitive ratios show good agreement.

The ground $^2$P levels do not come into Boltzmann equilibrium until around $10^{10}$ cm$^{-3}$ and we have two useful ratios presented in Table 8 involving lines close in wavelength. Both ratios give consistent densities with the 356.03/347.41 ratio giving smaller error bars on account of greater sensitivity to the electron density.

### *9.5. S XII*

Only the $^2$P – $^2$D transitions fall within the SERTS-89 wavelength range, and two of the three were detected. The $^2P_{3/2}$ – $^2D_{3/2,5/2}$ transitions are separated enough in wavelength to be resolved, but the component at 299.79 is not reported by Thomas & Neupert; it is related to the 288.40 Å line by the branching ratio given in Table 6 from which an intensity of 15 erg cm$^{-2}$ s$^{-1}$ sr$^{-1}$ can be estimated, significantly below the SERTS-89 3$\sigma$ sensitivity limit of 53 erg cm$^{-2}$ s$^{-1}$ sr$^{-1}$ there.

299.53/288.40 is an excellent density diagnostic showing strong variation over $10^9$ – $10^{11}$ cm$^{-3}$ and the SERTS-89 intensities give a value of $10^{9.5}$ cm$^{-3}$ as shown in Table 8.

**Table 8.** Density sensitive line ratios for the B-like ions.

| Ion | Ratio | SERTS-89 | Log $N_e$ |
|---|---|---|---|
| Mg VIII | 315.02 / 313.74 | $3.2 \pm 0.6$ | $\geq 8.5$ |
| | 436.73[s]/ 430.45 | $1.04 \pm 0.27$ | $8.6^{+hi}_{-0.5}$ |
| Al IX | 392.41[s]/ 385.02 | $2.2 \pm 0.7$ | $\geq 8.8$ |
| | 305.09 / 282.43 | $0.61 \pm 0.39$ | $9.8^{+hi}_{-lo}$ |
| | 300.56 / 282.43 | $1.08 \pm 0.64$ | $\geq 8.3$ |
| Si X | 258.37 / 261.05 | $2.7 \pm 0.7$ | $9.1^{+0.8}_{-0.5}$ |
| | 356.03[s]/ 347.41 | $1.0 \pm 0.3$ | $9.1^{+0.3}_{-0.3}$ |
| S XII | 299.53 / 288.40 | $0.35 \pm 0.15$ | $9.5^{+0.2}_{-0.3}$ |

### *9.6. Summary*

The B-like ions from magnesium to sulphur provide useful density diagnostics for typical coronal densities, and the agreement with theory for the density insensitive ratios is generally excellent.

- Some spectral lines show problems: Ne VI 433.16 Å and 435.63 Å, and Mg VIII 430.45 Å and 436.73 Å, which may be due to possible errors in the intensity calibration curve for the 430–450 Å spectral range.
- There are some problems with the Al IX transitions which may result from blending as these lines are all fairly weak.
- The Si X 356.03/347.41 and S XII 299.53/288.40 ratios are recommended for density diagnostic work as they involve lines close in wavelength, are highly sensitive, and give densities consistent with other ions formed at similar temperatures.

## 10. Carbon iso-electronic sequence

The main EUV lines emitted by the C-like ions in the SERTS-89 spectral range originate from 2s–2p excitations of the ground 2s configuration. There are three main groups of lines that represent excitations from the $^3$P levels up to the $^3$S, $^3$P and $^3$D levels. For ions higher than magnesium the ground $^3$P levels come into Boltzmann equilibrium at coronal densities, so there exist useful density diagnostic ratios involving lines within these groups. For the lower ions, density diagnostics need to involve a line from one of these groups together with one of either the $^1$D–$^1$D or $^1$D–$^1$P transitions, the latter generally lying close in wavelength to the $^3$P–$^3$S transitions, while the former lie closer to the $^3$P–$^3$P transitions.

### *10.1. O III*

The two transitions reported in the Thomas & Neupert catalogue are 2p–3s transitions and are found at 374.05 Å and 374.16 Å (the 2s–2p transitions lie above 500 Å). CHIANTI, however, predicts a total of six lines in the 373–375 Å region at 373.80 Å, 374.01 Å, 374.08 Å, 374.16 Å, 374.33 Å and 374.44 Å. There are further complications, since N III lines are predicted at 374.20 Å, 374.43 Å and 374.44 Å, as well as a second order line of Fe XII at 373.77 Å!

To resolve this mess of lines, we will match the CHIANTI 374.08 Å line to the observed 374.05 Å line, and assume that the observed 374.16 Å line is a blend of the CHIANTI O III 374.16 Å and N III 374.20 Å lines.

With these identifications we can then make estimates of the other O III line intensities from the branching ratios and density insensitive ratios given in Tables 9 and 10. We note that the 373.80/374.05 ratio then predicts an intensity for the 373.80 Å line of around 5 erg $cm^{-2}\,s^{-1}\,sr^{-1}$. This is used later in Sect. 13.4 on Fe XII.

### *10.2. Ne V*

Three Ne V lines are reported in the SERTS-89 catalogue, although CHIANTI predicts another two lines at 357.95 Å and 365.60 Å. The 357.95 Å line is most likely a blend of the feature measured at 357.89 Å and identified by Thomas & Neupert as Ne IV. With the branching ratio in Table 9 we estimate a Ne V contribution of 5.3 erg $cm^{-2}\,s^{-1}\,sr^{-1}$; however, this then implies a rather small Ne IV contribution to the observed total of 7.8 erg $cm^{-2}\,s^{-1}\,sr^{-1}$. The remaining branching ratio, 358.46/359.38, is in excellent agreement with observations.

The predicted 365.60 Å line is important as it shows strong density sensitivity relative to the 359.38 Å line. A Fe X line is reported in the catalogue at 365.57 Å and is stronger than theory predicts, suggesting a blend (see Sect. 13.2 on Fe X). Assuming the extra component is due to Ne V, we can estimate an intensity of 11 erg $cm^{-2}\,s^{-1}\,sr^{-1}$ from the Fe X branching ratio given in Table 18. As a check on this we note that the 365.60/416.21 ratio is density insensitive, with a theoretical value given in Table 10 predicting a Ne V component of around 13 erg $cm^{-2}\,s^{-1}\,sr^{-1}$ in excellent agreement with the previous estimate.

Either of the 365.60/359.38 and 416.21/359.38 ratios can be used as a density diagnostic as the 359.38 Å line is principally excited from the $^3$P levels, whereas the 365.60 Å and 416.21 Å lines are excited from the $^1$D level, which comes into Boltzmann equilibrium at around $10^{9.5}\,cm^{-3}$. We use the 416.21/359.38 ratio to derive a density of $10^{7.9}\,cm^{-3}$, considerably lower than expected. We note that if the calibration scale is altered as suggested in Sect. 15.1, the predicted density becomes $10^{8.3}\,cm^{-3}$.

### *10.3. Mg VII*

The $^3$P ground levels are in Boltzmann equilibrium for densities in the range $10^8 - 10^{12}\,cm^{-3}$ so all lines excited from these levels will be density insensitive relative to each other. The strongest lines emitted from the multiplets 2s2p $^3$S, $^3$P and $^3$D are 278.41 Å, 367.68 Å (which is a blend of two Mg VII lines) and 434.92 Å, respectively. A comparison of the SERTS-89 observations of these lines with theory is reported in Table 10.

**Table 9.** Branching ratios for the C-like ions.

| Ion | Ratio | Theory | SERTS-89 |
|---|---|---|---|
| O III | 374.00[n]/ 374.16 | 1.33 | – |
| | 374.44[n]/ 374.16 | 1.67 | – |
| | 373.80[i]/ 374.05 | 0.33 | – |
| Ne V | 357.95[n]/ 359.38 | 0.20 | – |
| | 358.46 / 359.38 | 0.60 | $0.58 \pm 0.17$ |
| Mg VII | 276.14[n]/ 278.41 | 0.20 | – |
| | 277.05 / 278.41 | 0.59 | – |
| | 431.14 / 429.13 | 0.64 | $0.84 \pm 0.34$ |
| | 434.69 / 431.29 | 0.24 | $0.13 \pm 0.08$ ◁ |
| Si IX | 344.96 / 341.97 | 0.57 | $0.59 \pm 0.17$ |
| S XI | 186.88[b]/ 191.23 | 0.20 | $4.7 \pm 2.5$ ◁ |
| | 247.16[i]/ 239.83 | 1.13 | $0.65 \pm 0.42$ ◁ |
| | 285.58 / 281.44 | 0.49 | $1.47 \pm 0.81$ ◁ |

The 278.41 Å line is clearly seen to be discrepant with theory. This can be partly explained by a Si VII line not identified by Thomas & Neupert that is predicted to lie at 278.44 Å. From Sect. 12.3, we can estimate a contribution of around 34 erg $cm^{-2}\,s^{-1}\,sr^{-1}$ for the Si VII component, but this still leaves approximately 46 erg $cm^{-2}\,s^{-1}\,sr^{-1}$ of the 278.41 Å line unaccounted for.

Estimating the 278.41 Å intensity as 34 erg $cm^{-2}\,s^{-1}\,sr^{-1}$ (deduced from the 367.68/278.41 insensitive ratio whose theoretical value is given in Table 10), we can estimate a Mg VII contribution to the 277.05 Å blend of 20 erg $cm^{-2}\,s^{-1}\,sr^{-1}$ from the branching ratio presented in Table 9. This estimate of the Mg VII contribution to 277.05 Å is used later in Sect. 11.3 on Si VIII. We also give in Table 9 the branching ratio involving the 276.14 Å line, which is not identified in the catalogue.

Dwivedi et al. (1997) report the identification of the CHIANTI 276.14 Å line in the SERTS-89 spectrum at 276.148 Å, and the full details of this fit are given in Table 24. We note that the intensity of this feature would then imply that the original 278.41 Å intensity of 114 erg $cm^{-2}\,s^{-1}\,sr^{-1}$ is correct, in contradiction of the above discussion. We thus suggest that the 276.148 Å is a blend to which Mg VII provides a component.

The insensitive 434.92/367.68 ratio is inconsistent with theory, with the 434.92 Å line seeming too weak. Again, this may simply reflect a problem with the instrumental calibration, although the extent of the discrepancy is not as marked as it is for Ne VI or Mg VIII, say.

The theoretical branching/density-insensitive ratios among the 360–370 Å and 429–435 Å lines show reasonable agreement with observations; in particular, discrepancies among the 429–435 Å lines are small. The line at 434.69 Å was not reported in the Thomas & Neupert catalogue but has subsequently been

**Table 10.** Insensitive ratios for the C-like ions.

| Ion | Ratio | Theory | SERTS-89 |
|---|---|---|---|
| O III | 374.16[b]/ 374.05 | 0.19 | $0.34 \pm 0.24$ |
| | 374.33[n]/ 374.05 | 0.27 | – |
| Ne V | 365.60[b]/ 416.21 | $0.54 \pm 0.05$ | $1.8 \pm 0.4$ |
| Mg VII | 278.41 / 367.68[s] | $0.76 \pm 0.03$ | $2.5 \pm 0.6$ ◁◁ |
| | 363.75 / 367.68[s] | 0.19 | $0.24 \pm 0.07$ |
| | 365.21[s]/ 367.68[s] | $0.60 \pm 0.01$ | $0.50 \pm 0.11$ |
| | 434.92 / 367.68[s] | $0.79 \pm 0.02$ | $0.60 \pm 0.11$ ◁ |
| | 429.13 / 434.92 | $0.27 \pm 0.01$ | $0.39 \pm 0.10$ ◁ |
| | 431.29 / 434.92 | $0.60 \pm 0.03$ | $0.63 \pm 0.15$ |
| Si IX | 292.80[s]/ 290.69 | $3.1 \pm 0.1$ | $2.1 \pm 1.1$ |
| | 296.13 / 292.80[s] | $1.32 \pm 0.02$ | $2.07 \pm 0.65$ ◁ |
| | 296.23 / 292.80[s] | 0.38 | $0.48 \pm 0.39$ |
| | 345.13 / 341.97 | $2.27 \pm 0.06$ | $2.41 \pm 0.52$ |
| | 349.87[s]/ 345.13 | $1.75 \pm 0.03$ | $1.97 \pm 0.36$ |
| | [345,349] / [292,296]† | $0.93 \pm 0.02$ | $0.84 \pm 0.15$ |
| S XI | 191.23 / [242]‡ | $1.82 \pm 0.29$ | – |

† [345,349] refers to the sum of the observed 345.13 Å and 349.87 Å lines, while [292,296] refers to the sum of the 292.80 Å, 296.13 Å and 296.23 Å lines.
‡ A blend of two lines predicted by CHIANTI at 242.85 Å and 242.87 Å.

**Table 11.** Density sensitive line ratios for the C-like ions.

| Ion | Ratio | SERTS-89 | Log $N_e$ |
|---|---|---|---|
| Ne V | 416.21 / 359.38 | $0.92 \pm 0.20$ | $7.9^{+0.2}_{-0.2}$ |
| Mg VII | 280.75[i]/ 367.68[s] | $0.20 \pm 0.16$ | $9.1^{+0.5}_{-1.1}$ |
| | 319.02[c]/ 367.68[s] | $1.10 \pm 0.27$ | $10.5^{+hi}_{-0.6}$ |
| Si IX | 296.13 / 296.23 | $4.3 \pm 3.4$ | $\geq 8.5$ |
| | 292.80 / 290.69 | $2.1 \pm 1.1$ | $7.5^{+hi}_{-lo}$ |
| | 296.23 / 292.80 | $0.48 \pm 0.39$ | $8.0^{+hi}_{-lo}$ |
| | 345.13 / 341.97 | $2.41 \pm 0.52$ | $\geq 8.6$ |
| | 349.87 / 345.13 | $1.97 \pm 0.36$ | $\geq 9.4$ |
| | 258.10 / 296.13 | $0.34 \pm 0.15$ | $9.8^{+0.2}_{-0.4}$ |
| S XI | 246.89 / 191.23 | $0.36 \pm 0.23$ | $8.7^{+0.6}_{-lo}$ |
| | 246.89 / 247.16 | $1.22 \pm 0.79$ | $9.0^{+0.4}_{-0.9}$ |
| | 285.83 / 281.44 | $1.88 \pm 0.95$ | $9.9^{+hi}_{-0.9}$ |

fitted. The details of the transition and fitted profile are provided in Table 24.

The $^1$D–$^1$D and $^1$D–$^1$P transitions mentioned earlier occur at 319.03 Å and 280.74 Å in CHIANTI and ratios taken relative to lines principally excited from $^3$P levels are sensitive to densities below around $10^{10}$ cm$^{-3}$. Of this pair, the SERTS-89 catalogue identified only the line at 319.02 Å which is blended with a Ni XV transition. Dwivedi et al. (1997) give a fit to a line at 280.749 Å (which we reproduce in Table 24) and suggest that it is the other Mg VII transition. We give in Table 11 the predicted density from the 280.75/367.68 ratio. An estimate of the Mg VII contribution to the line at 319.02 Å is made in Sect. 14.2, and we use this value of 51 erg cm$^{-2}$ s$^{-1}$ sr$^{-1}$ in the 319.02/367.68 ratio to give the density in Table 11.

### *10.4. Si IX*

The $^3$P–$^3$S transitions are found in the 220–230 Å region and so were not observed by SERTS-89. Only the one branching ratio (344.96/341.97) can be resolved in the spectrum and it gives excellent agreement with observations – see Table 9.

The line reported in the catalogue at 296.137 Å is identified as a blend of two Si IX transitions, which CHIANTI gives at 296.11 Å and 296.23 Å so making them potentially separable. Indeed, careful analysis of the SERTS-89 feature at 296.137 Å does reveal two components which we identify as the two Si IX lines. Details of these newly fitted profiles are listed in Table 24. The two components are density sensitive relative to each other, and we obtain an lower limit to the density, shown in Table 11.

The ground $^3$P levels do not approach Boltzmann equilibrium until around $10^9$ cm$^{-3}$ and so we find density sensitivity amongst lines within the three groups mentioned earlier. Such ratios are most useful for quiet Sun and coronal hole observations where we expect densities lower than $10^9$ cm$^{-3}$. This density sensitivity makes it difficult to identify density insensitive ratios appropriate for the SERTS-89 spectrum, but one solution is to sum together groups of lines, allowing the different degrees of sensitivity to cancel out. One such example is to sum the 292.80 Å, 296.13 Å and 296.23 Å lines and take the ratio relative to the sum of the 344.96 Å, 345.13 Å and 349.87 Å lines. We list this ratio in Table 10 and agreement is found within the error bars on the data.

For individual lines, we can check to see if the observed ratios lie close to their high density limit, as expected. Taking five ratios – 292.80/290.69, 296.13/292.80, 296.23/292.80, 345.13/341.97 and 349.87/345.13 – we display a comparison with theory in Table 10, the theoretical value being the average of the ratio over the $10^{9.5}$ – $10^{12}$ cm$^{-3}$ density regime – essentially the high density limit. Four of the ratios agree within the error bars on the data, while the 296.13/292.80 ratio lies marginally above the high density limit. In Table 11 we display the four ratios that agree with theory, but this time give the densities that they predict.

Only one of the two lines excited from the ground $^1$D level is observed in the SERTS-89 spectrum at 258.095 Å (the $^1$D – $^1$D transition) and it provides a good density diagnostic for densities $10^{9.5}$ – $10^{12}$ cm$^{-3}$ when taken relative to any line excited from the ground $^3$P levels. We choose to use the strong 296.13 Å line, leading to the estimated density shown in Table 11.

### *10.5. S XI*

Lines from all of the three groups mentioned previously are seen in the SERTS-89 spectrum although the error bars on the lines are rather large due to low instrumental efficiency at these wavelengths: the $^3$P–$^3$S lines are seen in second order, while the $^3$P–$^3$P and $^3$P–$^3$D lines lie towards the short wavelength end of

the bandpass. Two lines are reported as blended – 186.88 Å and 191.23 Å – although the Fe XIII line at 191.23 Å is expected to contribute very little (see Sect. 13.5 on Fe XIII). S XI contributes only a weak component to the 186.88 Å line, as witnessed by the 186.88/191.23 branching ratio presented in Table 9. We estimate a S XI contribution of 55 erg $cm^{-2}\,s^{-1}\,sr^{-1}$, just 4% of the total. The observed 285.58/281.44 ratio shows a discrepancy with theory and we suggest that the 285.58 Å line is blended with another (unknown) line. The 247.16/239.83 branching ratio indicates that we would expect a line at 247.16 Å which was not reported by Thomas & Neupert. Re-analysis of the SERTS-89 spectrum does show a line at this wavelength with an intensity which is just $1\sigma$ from the predicted value. Details of this new fit are given in Table 24.

The ground $^3$P levels come into Boltzmann equilibrium at $10^{10} - 10^{11}$ $cm^{-3}$ which makes for many potentially good density diagnostics, but limits the number of density insensitive ratios that are available. CHIANTI does predict a pair of lines at 242.85 Å and 242.87 Å, not seen in the SERTS-89 spectrum, which are density insensitive relative to the 191.23 Å line. The latter is identified as a blend with Fe XIII, but even if it were due entirely to S XI, the calculated ratio shown in Table 10 then implies the 242.85/7 blend would have an expected intensity of no more than around 157 erg $cm^{-2}\,s^{-1}\,sr^{-1}$. Thus the non-detection by SERTS-89 is quite reasonable, since its $3\sigma$-sensitivity limit is 225 erg $cm^{-2}\,s^{-1}\,sr^{-1}$ at that wavelength. However, this predicted blend might be observable by future, more efficient instruments. No other useful density-insensitive ratios exist at these wavelengths for S XI.

There are a number of potentially excellent density diagnostic ratios, including 247.16/246.89, 281.44/291.58 and 285.58/285.83. However, the 285.58 Å line needs to be used with care since it may be affected by blending as mentioned above. Although the 291.58 Å line was not seen by SERTS-89, we can use the $3\sigma$ spectral sensitivity level to estimate an upper limit of 55 erg $cm^{-2}\,s^{-1}\,sr^{-1}$ for its intensity, which implies a density value of $\leq 9.7$. The other measured ratios also give reasonable densities within their error bars, as shown in Table 11.

The $^1$D – $^1$D transition gives rise to a line at 215.97 Å and so would be seen in second order at around 431.94 Å but it is not reported in the catalogue. Since the line is predicted to gain significant intensity only above $10^{11}$ $cm^{-3}$ this is as expected.

### *10.6. Summary*

The C-like ions provide many potentially excellent density diagnostics, and comparisons with the SERTS-89 spectrum show reasonably consistent results in general. However, a few problems were encountered that point out the need for some caution when using these diagnostics, as follows.

- The Ne V 416.21/359.38 ratio gives a surpisingly low density of around $10^{7.9}$ $cm^{-3}$
- The most useful Mg VII line for density work is 319.02 Å, but it is blended with a Ni XV line making interpretation difficult.
- For Si IX many of the density diagnostics are useful only for quiet Sun or coronal hole studies. The 258.10 Å line can be used for active region work, however. In particular, the ratio 258.10/296.14 gives a density in good agreement with other ions.
- There are several problems with the S XI lines which may be due to blending. Still, this ion has a number of ratios that are potentially very useful as density diagnostics, especially for solar active regions, if used with proper care.

## 11. Nitrogen iso-electronic sequence

There are three main groups of $2s^22p^3 - 2s2p^4$ transitions which can be observed at SERTS-89 wavelengths, namely $^4$S – $^4$P, $^2$D – $^2$D and $^2$D – $^2$P. There are also three groups of weaker lines decaying down from the $^2$D, $^2$P and $^2$S levels to the $^2$P levels in the ground state, with the $^2$P – $^2$S transitions being the strongest of those.

### *11.1. Ne IV*

The $^4$S – $^4$P and $^2$D – $^2$D transitions occur above 450 Å and so are not observed by SERTS-89. Subsequently, we only have two Ne IV lines identified (357.89 and 421.59 Å), both of which are weak. Dwivedi et al. (1997) suggest the identification of a line at 388.228 Å, and we give the details of the line fit and transition in Table 24.

CHIANTI predicts the strongest Ne IV line to occur at 358.68 Å, but it is not reported in the catalogue. However, a Fe XI line is identified at 358.67 Å and, as explained in Sect. 13.3, the intensity is too strong to be accounted for by Fe XI alone. We suggest that Ne IV is a significant component of this feature, and can estimate its contribution as follows. As shown in Sect. 10.2, Ne IV accounts for 2.5 erg $cm^{-2}\,s^{-1}\,sr^{-1}$ of the blend with Ne V at 357.95 Å. Using this and the density insensitive ratio given in Table 13 for 357.89/358.68, we then get a Ne IV contribution of 5 erg $cm^{-2}\,s^{-1}\,sr^{-1}$ to the 358.67 Å blend.

The 388.23/357.89 ratio is also density insenstive, and the revised value for the 357.89 Å intensity ensures that the ratio agrees well with theory (Table 13).

The line at 421.59 Å is a self-blend excited principally from the ground $^2$P levels and so shows density sensitivity relative to the 357.89 Å line up to around $10^9$ $cm^{-3}$ when the $^2$P levels come into Boltzmann equilibrium with the $^2$D levels. Although this ratio is more useful for lower density sources, we note that the intensity ratio observed by SERTS-89, as corrected above, is consistent with the expected high-density limit predicted by CHIANTI and shown in Table 14.

### *11.2. Mg VI*

The three groups of strong lines mentioned in the introduction are all present in the SERTS-89 spectrum. In addition, Thomas & Neupert identified a SERTS-89 feature at 319.73 Å as the $2s2p^4\ ^2D_{3/2} - 2p^5\ ^2P_{1/2}$ transition which is not included in the CHIANTI atomic model. However, that line is principally

**Table 12.** Branching ratios for the N-like ions.

| Ion | Ratio | Theory | SERTS-89 |
|---|---|---|---|
| Mg VI | 293.15[i,s]/ 270.40[s] | 0.22 | $0.24 \pm 0.15$ |
| | 291.36[i,s]/ 269.04 | 0.32 | $0.28 \pm 0.21$ |
| | 314.56[n]/ 314.67[n] | 0.57 | – |

**Table 13.** Insensitive ratios for the N-like ions.

| Ion | Ratio | Theory | SERTS-89 |
|---|---|---|---|
| Ne IV | 357.89 / 358.67[i] | $0.54 \pm 0.01$ | – |
| | 388.23[n]/ 357.89 | $0.52 \pm 0.01$ | $0.56 \pm 0.44$ |
| Mg VI | 269.04 / 270.40[s] | $0.46 \pm 0.01$ | $0.63 \pm 0.34$ |
| | 270.40[s]/ 349.16[s] | $0.52 \pm 0.06$[T] | $1.07 \pm 0.35$ ◁ |
| | 387.77[i]/ 387.97[i] | $0.56 \pm 0.03$ | $0.61 \pm 0.33$ |
| | 387.97[i]/ 349.16[s] | $0.085 \pm 0.002$ | $0.11 \pm 0.05$ |
| | 399.28 / 400.67 | 0.53 | $0.57 \pm 0.14$ |
| | 403.30[c]/ 400.67 | $1.47 \pm 0.01$ | $1.67 \pm 0.43$ |
| Si VIII | 216.94[i]/ 277.05 | $1.00 \pm 0.07$[T] | $0.51 \pm 0.44$ |
| | 314.35 / 319.84 | 0.35 | $0.48 \pm 0.15$ |
| | 316.22 / 319.84 | 0.66 | $0.78 \pm 0.20$ |
| S X | 257.15[i]/ 264.22 | 0.35 | $0.30 \pm 0.21$ |
| | 259.50 / 264.22 | 0.67 | $1.28 \pm 0.62$ |

excited by very weak transitions from the ground levels and is not likely to have a significant intensity, so we can rule out this identification.

There are two relatively strong $^2$P – $^2$D transitions predicted by CHIANTI at 387.79 Å and 388.01 Å, whereas Thomas & Neupert reported only one broad feature at 387.95 Å that they identified as the second of these lines. We now find that both lines can be measured in the SERTS-89 spectrum with wavelengths of 387.769 Å and 387.967 Å. Other details of the fits can be found in Table 24. The two lines are density insensitive relative to each other and also with the 349.16 Å line. We present comparisons with theory in Table 13, where good agreement is found.

The line at 403.30 Å is blended with a Ne VI transition (see Sect. 9.1), and we can use a Ne VI branching ratio to estimate the Mg VI contribution as around 27 erg cm$^{-2}$ s$^{-1}$ sr$^{-1}$. We use this value in Table 13 where it shows excellent agreement with the 400.67 Å line. We also find the 399.28/400.67 ratio to be in agreement with theory.

The two $^2$D – $^2$P transitions at 269.04 Å and 270.40 Å are density insensitive relative to each other and show agreement with theory (Table 13). However when compared with the $^2$D – $^2$D transitions which are self-blended at 349.16 Å – we find a discrepancy as witnessed by the 270.40/349.16 ratio. The 349.16 Å self-blend seems too low in intensity by about 30 – 40%.

Taking the ratio of the $^2$D – $^2$D transitions to the $^4$S – $^4$P transitions potentially yields a good density diagnostic over $10^7$ – $10^{10}$ cm$^{-3}$. However, if we take the 349.16/400.67 ratio, for example, the high density limit is around 2.3 and yet the observed ratio is $3.4 \pm 0.7$, suggesting either that the $^4$S – $^4$P transitions are too weak in the SERTS-89 spectrum or that the 349.16 Å self-blend is too strong. (Note that the latter possibility is in direct conflict with the conclusion drawn in the previous paragraph.)

Of further interest regarding density diagnostics are two lines predicted by CHIANTI at 314.56 Å and 314.67 Å, which are $^2$P – $^2$S transitions and related to each other by the branching ratio given in Table 12. Both lines are strongly density sensitive relative to 349.16 Å up to $10^{10}$ cm$^{-3}$, but neither are identified in the catalogue. However we do find an unidentified line at 314.59 Å, which Dwivedi et al. (1997) identify as the CHIANTI 314.67 Å line. We note that the 314.67/349.16 ratio has an upper limit of 0.15, yet the observed 314.59/349.16 ratio is $0.29 \pm 0.12$, marginally above this value. Another possibility is that the CHIANTI 314.56 Å and 314.67 Å lines are blended in the SERTS-89 spectrum, but the separation of the lines is governed by the separation of the ground configuration $^2$P levels which is strongly constrained by observations of ultra-violet lines at 1190.1 Å and 1191.7 Å. Thus SERTS-89 should be capable of resolving these lines. On account of the above we can not confirm the identification of Dwivedi et al. (1997), and we await further high resolution spectra of this wavelength region.

Dwivedi et al. (1997) give two additional Mg VI identifications at 291.359 Å and 293.146 Å, and we give details of the line fits and transitions in Table 24. Both lines are blends of two Mg VI transitions, and they are related to the 269.04 Å and 270.40 Å lines, respectively, via branching ratios. Comparisons with theory are presented in Table 13, where good agreement is found.

The problems noted in comparing the $^2$D – $^2$P, $^2$D – $^2$D and $^4$S – $^4$P transitions seem likely to be due to inaccuracies in the Mg VI atomic data adopted for CHIANTI. Since there are very few calculations of collision rates and transition probabilities available in the literature, future studies would be highly desirable for this ion.

### *11.3. Si VIII*

The 338.38 Å line identified in the SERTS-89 catalogue is a $2s2p^4$ – $2p^5$ transition and so is not in the CHIANTI model of Si VIII. However, for the same reason as with the Mg VI $2s2p^4$ – $2p^5$ transition, we dismiss this identification. The other reported transitions come from the $^4$S – $^4$P and $^2$D – $^2$D multiplets.

The 277.05 Å line is reported as blended with a Mg VII transition and from Sect. 10.3 we can estimate the Si VIII contribution to be around 60 erg cm$^{-2}$ s$^{-1}$ sr$^{-1}$. Although not reported, the 276.85 Å line is expected to be blended with a Si VII transition and from Sect. 12.3 we estimate a Si VIII contribution of 45 erg cm$^{-2}$ s$^{-1}$ sr$^{-1}$. As the two ground $^2$D levels come into Boltzmann equilibrium with the $^4$S level at different densities, the 276.85/277.05 ratio is sensitive to densities up to around $10^{9.5}$ cm$^{-3}$. With the "de-blended" intensities we find the ratio close to the high density limit and we give the density estimate in Table 14.

**Table 14.** Density sensitive line ratios for the N-like ions.

| Ion | Ratio | SERTS-89 | Log $N_e$ |
|---|---|---|---|
| Ne IV | 421.59[s]/ 357.89[c] | $1.7 \pm 1.0$ | $\geq 8.2$ |
| Si VIII | 276.85[c]/ 277.05[c] | $0.75 \pm 0.41$ | $9.3^{+hi}_{-1.1}$ |
| | 277.05[c]/ 319.84 | $0.53 \pm 0.21$ | $10.4^{+0.6}_{-0.9}$ |

**Table 15.** Branching ratios for the O-like ions.

| Ion | Ratio | Theory | SERTS-89 |
|---|---|---|---|
| Ne III | 427.84 / 379.31 | 0.059 | $0.51 \pm 0.28$ ◁◁ |
| Mg V | 355.34 / 353.08 | 0.33 | $1.09 \pm 0.72$ ◁ |
| | 353.29[b]/ 351.12 | 0.59 | $0.77 \pm 0.36$ |
| | 354.16 / 351.12 | 0.77 | $0.69 \pm 0.43$ |
| Si VII | 275.62[i]/ 272.56[i] | 0.57 | $1.13 \pm 1.04$ |
| | 278.41[i]/ 275.38 | 0.32 | – |

The three $^4$S – $^4$P transitions that occur at 314–320 Å are density insensitive relative to each other, and comparisons with theory provided in Table 13. Reasonable agreement is found.

Comparing either of the $^2$D – $^2$D lines to one of the $^4$S – $^4$P lines yields a density diagnostic valid over the range $10^8$ – $10^{12}$ cm$^{-3}$. We choose the 277.05/319.84 ratio and use the "deblended" intensity for the 277.05 Å line to give the density shown in Table 14.

The $^2$D – $^2$P transitions, not reported by Thomas & Neupert, occur at around 216 Å and so lie in the second order bandpass of SERTS. Dwivedi et al. (1997) report a new identification for the Si VIII 216.92 Å line (the strongest of the $^2$D – $^2$P transitions) and details of the fit are given in Table 24. This line is density insensitive relative to the 277.05 Å line and we compare the observed ratio with theory in Table 13, where we have used the above intensity estimate of 60 erg cm$^{-2}$ s$^{-1}$ sr$^{-1}$ for the 277.05 Å line. The large error bars on the observations allow marginal agreement.

### *11.4. S X*

Only the $^4$S – $^4$P transitions fall within the SERTS-89 bandpass and of these only two of the three transitions are reported in the catalogue, although Dwivedi et al. (1997) have since reported the identification of the remaining transition, for which the fit details are given in Table 24. The three lines are all density insensitive relative to each other with values given in Table 13. The 259.45/264.22 ratio shows only marginal agreement with theory, suggesting that the 259.45 Å line may be blended, although we note that Malinovsky & Heroux (1973) give a value of 1.06 for this ratio in their full-disk solar spectrum, consistent with the SERTS value.

### *11.5. Summary*

The nitrogen sequence of ions potentially provide excellent density diagnostics, but for the lines in the SERTS-89 spectrum we are hampered by blending and inconsistencies in the atomic data.

- The Ne IV 421.59/357.89 ratio is very sensitive to densities below $10^9$ cm$^{-3}$, although observations need to be corrected for the 357.89 Å blend with Ne V.
- Mg VI shows inconsistencies in relatively comparing lines from the $^4$S – $^4$P, $^2$D – $^2$D and $^2$D – $^2$P transitions, although comparisons of lines within these multiplets shows good agreement with theory. The inconsistencies prevent a density estimate being made.
- For Si VIII, density diagnostics can be obtained from the two $^2$D – $^2$D transitions, and also by comparing these to the $^4$S – $^4$P transitions. However, both of the $^2$D – $^2$D lines are blended with lines from other species, making the density estimates uncertain.
- There are no S X density diagnostics available in the SERTS-89 waveband.

## 12. Oxygen iso-electronic sequence

In terms of the 2s – 2p transitions, the Oxygen-like ions are very simple: the $2s^22p^4$ $^3$P – $2s2p^5$ $^3$P transitions give rise to 6 closely spaced lines which, for the higher ions, show some relative density sensitivity. For the lower ions $2s^22p^4$ $^1$D – $2s2p^5$ $^1$P is usefully density sensitive relative to the $^3$P – $^3$P transitions.

### *12.1. Ne III*

The six $^3$P – $^3$P transitions lie at 488–491 Å and so fall outside the SERTS-89 bandpass. Of the four lines in the spectrum identified as Ne III, two involve transitions that originate from the $2p^3 3s$ configuration for which electron collisional excitation data are unavailable.

The remaining two transitions are related by branching ratio, as shown in Table 15. Clearly, the predicted Ne III line at 427.84 Å is far too weak to explain the intensity measured at this location, and we suggest this line belongs to another ion.

### *12.2. Mg V*

There are six transitions identified, but the 376.63 Å line cannot be the Mg V $2s2p^5$ $^1$P – $2p^6$ $^1$S transition since it is theoretically predicted to be around five orders of magnitude weaker than the 353.08 Å line. The remaining lines show a very weak relative density sensitivity, and are of no use as diagnostics. Tables 15 and 16 show that there seem to be problems with the 353.08 Å line, even taking into account the large error bars of the data. The intensity of this line seems to be too low compared with theory. The remaining lines are consistent.

For the 353.29 Å blend with Na VII, we can use Table 15 to estimate the Mg V portion as around 7 erg cm$^{-2}$ s$^{-1}$ sr$^{-1}$ of the total 10 erg cm$^{-2}$ s$^{-1}$ sr$^{-1}$.

Dwivedi et al. (1997) have identified an additional Mg V line at 276.600 Å and we give the fit and transition information in

**Table 16.** Insensitive ratios for the O-like ions.

| Ion | Ratio | Theory | SERTS-89 |
|---|---|---|---|
| Mg V | 351.12 / 353.08 | $0.32 \pm 0.01$ | $1.26 \pm 0.64$ ◁ |
| | 351.12 / 355.34 | $1.00 \pm 0.04$ | $1.16 \pm 0.76$ |
| | 352.21[i] / 351.12 | $0.80 \pm 0.02$ | $0.33 \pm 0.27$ ◁ |
| Si VII | 276.85[i] / 275.38 | $0.20 \pm 0.02$ | – |

**Table 17.** Density sensitive line ratios for the O-like ions.

| Ion | Ratio | SERTS-89 | Log $N_e$ |
|---|---|---|---|
| Mg V | 276.60 / 351.12 | $1.71 \pm 1.11$ | $9.6^{+hi}_{-1.2}$ |

Table 24. This line is the $^1D$ – $^1P$ transition mentioned earlier and shows density sensitivity relative to the $^3P$ – $^3P$ transitions. We give in Table 17 the density predicted from the observed 276.60/351.12 ratio.

Another Mg V line identified by Dwivedi et al. (1997) is at 352.213 Å and the details of the fit and transition are given in Table 24. This line is insensitive relative to the 351.12 Å line, but the observed intensity is lower than expected as can be seen in Table 16.

### *12.3. Si VII*

Only one transition of the $^3P$ – $^3P$ multiplet is seen at 275.38 Å, but another five weaker lines are expected in the 270–280 Å region. Two of these lines are predicted to provide components to observed lines at 276.85 Å and 278.41 Å (identified as Si VIII and Mg VII lines, respectively), and the Si VII components can be estimated from the 275.38 Å intensity of 105 erg $cm^{-2}$ $s^{-1}$ $sr^{-1}$ using the branching ratio and density insensitive ratio provided in Tables 15 and 16.

Of the remaining three transitions, the line expected at 274.17 Å is density dependent below $10^9$ $cm^{-3}$ relative to the 275.38 Å line, but unfortunately it is masked by the far stronger Fe XIV 274.21 Å and contributes no more than 3% to that feature. Dwivedi et al. (1997) give new identifications for the remaining two lines which CHIANTI predicts to be at 272.64 Å and 275.67 Å. The fits to these lines are given in Table 24, where we note that the wavelengths differ significantly from the CHIANTI values. The two lines are related to each other by the branching ratio given in Table 15, but the large error bars on the data make comparisons with theory meaningless. The 272.64/275.35 ratio shows mild density sensitivity, increasing from 0.20 to 0.29 over the density regime $10^8$ – $10^{12}$ $cm^{-3}$, with the observed value being $0.17 \pm 0.14$, agreeing reasonably with theory.

### *12.4. Summary*

The O-like ions give rise to weak lines in the EUV, which makes them difficult to use for diagnostic work.

- The 2p – 3s transitions of Ne III can not be modelled at present as no collisional data are available for these transitions.
- The potentially useful Mg V 276.58 Å line is expected to be quite weak, requiring a very high sensitivity instrument for detection. All of the observed Mg V lines are consistent with theory, with the exceptions of 353.08 Å which is weaker than predicted and 376.63 Å which must have been misidentified.
- Two unidentified Si VII lines are suggested to be blended with observed lines. No density diagnostics are available for this ion.

## 13. The Iron Ions

The iron ions are the most useful of the coronal ions as they retain many of their n=3 electrons at coronal temperatures and the resulting complexity of the ions ensures that there are many emission lines found in the EUV, including many potential density diagnostic line pairs. This complexity, however, also makes the iron ions difficult to model and so it is important to use solar emission line spectra as testing grounds for the atomic data as well as for plasma parameter determinations.

Brickhouse et al. (1995) have provided a comparison of theory with the SERTS-89 observations, and we refer to this work where appropriate. We note that the atomic data used by Brickhouse et al. (1995) are not identical to that found in the CHIANTI database – new calculations for Fe X and Fe XI have appeared since this work, for example – and we refer the reader to Paper I for details.

The Iron Project (Hummer et al. 1993) aims to provide improved data for all the iron ions and in particular the Fe IX–XVII ions looked at here. These data are, as yet, unavailable and so the current work summarises the "pre-Iron Project" status.

### *13.1. Fe IX*

Fe IX is argon-like and so has a single ground level. The first excited configuration is $3p^5 3d$ and the most important EUV emission lines of Fe IX come from decays from this configuration to the ground. These are the single allowed transition at 171.07 Å, the two intercombination transitions at 217.10 Å and 244.92 Å, and the forbidden transition at 241.75 Å.

All four lines are observed in the SERTS-89 spectrum, although the 171.07 Å and 217.10 Å lines are observed in second order, while the 241.75 Å and 244.92 Å lines are close to the low wavelength end of the SERTS-89 bandpass. Additionally, the 171.07 Å line is close to the end of the SERTS-89 second order bandpass as mentioned in Brickhouse et al., creating additional uncertainties in the line intensity. Despite this, we note that there is reasonable agreement with the spectrum of Behring et al. (1976) for the intensities of the four lines.

There is no strictly density insensitive ratio between these four lines, but we show the 244.92/171.07 ratio in Table 19 as the error bars on the observed data are larger than the theoretical variation of the ratio. Clearly the ratio is discrepant with theory

by a factor of between 2 and 7, with the 171.07 Å line being over-estimated by theory.

We form two density sensitive ratios that are displayed in Table 20 with predicted densities, although the large error bars on the data mean that the values suggest little more than that the three lines are in broad agreement with theory (in contrast with the 171.07 Å line), with perhaps the 217.10 Å line – seen in second order at 434.20 Å – being too weak compared to theory.

Inconsistencies with the Fe IX line intensities have been seen previously: Feldman (1992) has noted that the 241.75/244.92 ratio gave densities significantly higher than other species in flares observed by the S082A spectrograph on *Skylab*; while Laming et al. (1995) point out that the SERTS-89 spectrum, the Malinovsky & Heroux (1973) quiet Sun spectrum and an EUVE spectrum of the star Procyon all have the *same* intensity pattern for the 171.07 Å and intercombination lines. Feldman (1992) proposed that the flare observations could be explained by high temperature transient bursts during the flare which prevent the 241.75 Å line decaying before Fe IX has ionised. However, this does not explain the allowed/ intercombination line ratios being discrepant in quiet Sun conditions.

We suggest here that the discrepancies are due to the atomic model used by Fawcett & Mason (1991) not including the $3s3p^6 3d$ and $3s3p^5 3d^2$ configurations which may be significant in de-populating the metastable levels of the $3s^2 3p^5 3d$ configuration. Additionally the SSTRUCT data used in calculating the transition probabilities (see Paper I) predicted a $3s3p^5 3d^2\ ^5G_6$ level as being the 28th excited level of the ion. This level has no allowed transition connecting it to lower levels and so one would anticipate a significant population at coronal densities.

Bearing in mind these points, we recommend that the Fe IX line intensities should be interpreted with caution and that the 244.92/241.75 ratio should *not* be used for detailed density diagnostic work until further theoretical work is done on this ion.

### *13.2. Fe X*

Four Fe X lines are reported in the SERTS-89 catalogue, the strongest being 174.52 Å which is observed in second order. This line is density insensitive relative to the first order 345.74 Å line (although there is some temperature sensitivity) and a comparison with theory is presented in Table 19. We find marginal agreement with theory, but note that we require the first order Fe XI 349.04 Å line to contribute very little to the blend. In the following section we show that this is not the case, and that it actually contributes around 50% to the blend.

The 365.57/345.74 branching ratio does not agree with observations (Table 18) and we believe that this is due to an unreported blend of the 365.57 Å line with Ne V 365.60 Å. Indeed, if we assume the extra flux in the 365.57 Å line is due to Ne V, then we find excellent agreement amongst the Ne V lines, as described in Sect. 10.2.

The line reported at 257.26 Å is actually a blend of two Fe X lines: the reported $^2P_{3/2}$–$^4D_{5/2}$ transition and the $^2P_{3/2}$–$^4D_{7/2}$ transition. The 345.74/257.26 ratio is density sensitive and the measured density is given in Table 20.

The Bhatia & Doschek (1995) calculations used in CHIANTI are the first to include electron excitation data for the $3s3p^5 3d$ configuration, and there are a host of weak lines excited from the metastable levels in the $3s^2 3p^4 3d$ configuration predicted in the 250–400 Å region. All of these are predicted weaker than the observed 345.74 Å line and many have never been observed. We draw attention to two transitions for which we do have observed wavelengths: 324.76 Å and 353.44 Å, both of which are density sensitive relative to 345.74 Å with relative intensities of around 0.1–0.3 in the density regime $10^9$–$10^{10}$ cm$^{-3}$. Such intensities make the lines potentially observable by SERTS-89, but neither are reported in the catalogue. We feel that, because of this, the Bhatia & Doschek (1995) data over-estimate the strength of these $3s^2 3p^4 3d$–$3s3p^5 3d$ transitions, due to limitations of the 4 configuration model for Fe X.

### *13.3. Fe XI*

The SERTS-89 catalogue lists an unidentified line at 406.791 Å that Brickhouse et al. identify as being the $3s^2 3p^4\ ^1D_2$ – $3s3p^5\ ^3P_2$ transition of Fe XI, which is then related to the 352.67 Å line by a branching ratio. The comparison with theory presented in Table 18 shows good agreement, as do the 356.63/341.11 and 369.16/352.67 ratios. However, there is a major discrepancy for the 358.67/341.11 ratio, with the 358.67 Å line being around a factor of 3 too strong. We attribute this to blending and there are two candidates suggested by CHIANTI. One was discussed in Sect. 8.3 as being due to Si XI with a predicted wavelength of 358.65 Å and intensity of around 14 erg cm$^{-2}$ s$^{-1}$ sr$^{-1}$; the other is a Ne IV line at 358.69 Å with an intensity of about 5 erg cm$^{-2}$ s$^{-1}$ sr$^{-1}$ as described in Sect. 11.1. Another line, not in the CHIANTI database, but suggested by Bhatia et al. (1994), is a line of Fe XIV which we estimate from their paper to have an intensity of around 5–20 erg cm$^{-2}$ s$^{-1}$ sr$^{-1}$. With our prediction that the Fe XI component should be near 24 erg cm$^{-2}$ s$^{-1}$ sr$^{-1}$, the observed intensity at 358.67 Å of 72.6 erg cm$^{-2}$ s$^{-1}$ sr$^{-1}$ seems to be well accounted for by a sum of these four lines.

Although the 341.11/352.67 ratio shows some density sensitivity, the variation of the ratio over $10^8$ – $10^{12}$ cm$^{-3}$ is of the same order as the error bars on the SERTS-89 data, and so we list this ratio in Table 19—good agreement is found with theory. The insensitive 352.67/188.21 ratio does not agree with theory, with the 188.21 Å line being apparently a factor of 2 too strong. This may be as a result of a blend of the second order line with a weak first order line. Note that one may have expected the strong 180.40 Å line to have been seen in the SERTS-89 spectrum in second order, however it is completely lost under the very intense Fe XVI 360.75 line.

Removing the redundancy provided by the density insensitive ratios, we are left with the two density sensitive ratios shown in Table 20. The 308.58/352.67 ratio gives a very high density which is at odds with results from other ions formed at the same temperature and may indicate that the 308.58 Å line is blended. Although the density derived from the 349.04/352.67 ratio seems more reasonable, we have not taken into account blending of the 349.04 Å line with second order Fe X 174.52 Å.

**Table 18.** Branching ratios for the iron ions

| Ion | Ratio | Theory | SERTS-89 |
|---|---|---|---|
| Fe X | 365.57 / 345.74 | 0.42 | $0.57 \pm 0.11$ ◁ |
| Fe XI | 356.53 / 341.11 | 0.50 | $0.40 \pm 0.15$ |
| | 358.67 / 341.11 | 0.64 | $1.95 \pm 0.39$ ◁◁ |
| | 369.16 / 352.67 | 0.30 | $0.29 \pm 0.05$ |
| | 406.79 / 352.67 | 0.027 | $0.022 \pm 0.009$ |
| Fe XII | 382.85 / 338.27 | 0.17 | $0.093 \pm 0.030$ ◁ |
| Fe XIII | 204.95 / 201.12[b] | 0.29 | $0.88 \pm 0.40$ ◁ |
| | 213.77 / 209.62 | 0.99 | $0.62 \pm 0.45$ |
| | 204.25 / 221.83 | 0.55 | $0.93 \pm 0.39$ |
| | 240.72 / 251.94 | 0.22 | $0.41 \pm 0.18$ ◁ |
| | 246.20 / 251.94 | 0.53 | $0.44 \pm 0.15$ |
| | 321.46 / 312.17 | 0.50 | $0.38 \pm 0.10$ ◁ |
| | 311.56 / 320.80 | 0.14 | $0.24 \pm 0.07$ ◁ |
| | 359.83 / 348.18 | 0.26 | $0.18 \pm 0.04$ ◁ |
| | 413.03 / 368.16[b] | 0.066 | $0.054 \pm 0.017$ |
| Fe XIV | 220.07 / 211.32 | 0.21 | $0.25 \pm 0.07$ |
| | 252.20 / 264.78 | 0.24 | $0.18 \pm 0.06$ |
| | 257.40 / 270.52 | 0.74 | $0.38 \pm 0.09$ ◁ |
| | 289.17 / 274.21 | 0.089 | $0.072 \pm 0.024$ |
| | 356.65 / 334.17 | 0.036 | $0.028 \pm 0.010$ |
| Fe XV | 312.54[b]/ 327.03 | 0.59 | $0.76 \pm 0.11$ |
| | 292.25[i]/ 304.87[b] | 0.37 | $0.21 \pm 0.07$ |
| Fe XVI | 265.02 / 251.07 | 0.16 | $0.19 \pm 0.06$ |

A lower estimate for the 349.04 Å intensity gives a lower density, and to be consistent with other density measurements we require Fe XI to contribute at least 50% to the blend at 349.04 Å.

### *13.4. Fe XII*

A detailed comparison of the SERTS-89 Fe XII line intensities with theory is provided in Keenan et al. (1996). We note that Keenan et al. use the electron collisional excitation calculations of Tayal & Henry (1988) for the 3s–3p transitions whereas for the CHIANTI database we retain the Flower (1977) calculations for these transitions, ensuring that we have a consistent set of data for the 3s–3p and 3p–3d transitions.

In the CHIANTI database we have used the recent laboratory identifications of Jupén et al. (1993) for some weak transitions of Fe X–XIV. One such identification was of a Fe XII line at 283.45 Å and indeed we find an unidentified line in the SERTS-89 spectrum at 283.486 Å. However, given this identification, we would then expect another line, related to 283.45 Å by a branching ratio, at around 312.29 Å. The 312.29/283.45 theoretical value is 0.42, implying a 312.29 Å intensity of 27 erg cm$^{-2}$ s$^{-1}$ sr$^{-1}$, yet this line is not reported.

Keenan et al. suggest that the Fe XII transition which CHIANTI puts at 283.45 Å is instead a weak feature at 283.70 Å (not reported in the original SERTS-89 catalogue; the fit to this feature is given in Table 24), and that the 283.49 Å line is actually due to N IV. We confirm that the 283.49 Å line is largely due to N IV, but it is still possible that Fe XII could be providing a weak component to this line. In Table 19 we give the theoretical value for the CHIANTI 283.45/338.27 ratio, which gives an indication of the likely intensity of the 283.45 Å line (the 338.27 Å intensity is 76.6 erg cm$^{-2}$ s$^{-1}$ sr$^{-1}$), but we note below that the 338.27 Å line blended. On account of the above discussion, we feel it is not possible to determine whether the CHIANTI 283.45 Å forms a component to the SERTS-89 283.49 Å feature, or whether it it actually occurs at 283.70 Å as suggested by Keenan et al. In the latter case, the low intensity is consistent with theory, but the wavelength disagrees with the laboratory work of Jupén et al. (1993).

Keenan et al. also suggest the identification of a line at 196.618 Å as being the $3p^3\ ^2D_{5/2}$ – $3p^2 3d\ ^2D_{5/2}$ transition. The measured intensity of this line on the old calibration scale (that used in the Thomas & Neupert paper) is $279 \pm 139$. A density insensitive ratio can be formed with the observed 219.43 Å line and a comparison with theory is shown in Table 19—the insensitivity has been assessed over $10^{8.5} - 10^{12}$ cm$^{-3}$. We have agreement with theory within the error bars, giving confidence in the identification, which we give in Table 24.

In the SERTS-89 spectrum, there is a Fe XII line identified at 335.04 Å but this transition in CHIANTI appears at 335.34 Å. This is because we have used the energy levels from Jupén et al. (1993) who have used a line at 376.405 Å to derive the energy for the $3s3p^4\ ^2D_{3/2}$ level, which gives rise to the line at 335.34 Å. We note, however, that the line at 376.405 Å is predicted to be around an order of magnitude weaker than the 335.34 Å line, which is in itself a weak line. This raises question marks over whether the 376.405 Å is really a Fe XII line, and so we will assume that the observed SERTS-89 line at 335.04 Å is in fact the identified Fe XII transition.

To take account of the weak Si XI line referred to in Sect. 8.3, we revise the 364.47 Å line intensity to 216 erg cm$^{-2}$ s$^{-1}$ sr$^{-1}$. This value is used in Tables 18 and 19.

Only one pair of lines in the observed Fe XII spectrum is related by branching ratio and we find a significant discrepancy with theory – see Table 18. As the observed ratio is lower than theory, we have to surmise that the 338.27 Å line may be blended.

Neither of the 200.41 Å and 201.12 Å lines is related to any other by a density insensitive line ratio, yet we believe that both lines are blended, by noting that taking either line relative to the 219.44 Å line yields a density diagnostic. However, neither line is predicted to be stronger than the 219.44 Å line at any density (the maximum values of the 200.41/219.44 and 201.12/219.44 ratios are 0.58 and 0.93, respectively), yet both lines are given significantly higher intensities in the catalogue.

For the 201.12 Å line, there is an identified blend with an Fe XIII line and from the following section on Fe XIII we have an estimate of the Fe XII contribution as 154 erg cm$^{-2}$ s$^{-1}$ sr$^{-1}$. This is still rather a large value and we suggest that there may be a very weak ($\sim$ 1–2 erg cm$^{-2}$ s$^{-1}$ sr$^{-1}$) first order line which may comprise some of the feature's measured response.

Keenan et al. suggest that the 200.41 Å line is blended with a weak first order Ca VI line, but we can not confirm this through

CHIANTI as Ca VI is not in the database. However, we can estimate the Fe XII contribution as at most 100 erg $cm^{-2}\,s^{-1}\,sr^{-1}$ and probably significantly less, compared to the SERTS-89 value of 365 erg $cm^{-2}\,s^{-1}\,sr^{-1}$.

Given the density insensitive 192.37/195.12 ratio in Table 19, we infer that it is the Mn XV 384.75 Å line that dominates the blend at 384.75 Å—the second order Fe XI 192.37 Å only contributing around 3–4 erg $cm^{-2}\,s^{-1}\,sr^{-1}$. The 193.51/195.12 ratio disagrees with theory: we suggest that the 193.51 Å line, seen in second order, may be blended with an unknown weak first order line.

The Fe XII line at 186.88 Å is a self-blend of the reported $3s^23p^3\ ^2D_{5/2} - 3s3p^4\ ^2F_{7/2}$ transition with the unreported $^2D_{3/2} - ^2F_{5/2}$ transition, and the 186.88/195.12 ratio is an excellent density diagnostic. A S XI line is also found at 186.88 Å, but, as stated in Sect. 10.5, it is expected to contribute around 55 erg $cm^{-2}\,s^{-1}\,sr^{-1}$ to the blend (only 4% of the total) and so could be neglected. On the other hand, CHIANTI predicts a weak first order O III line at 373.81 Å which, although expected to have an intensity of only around 5 erg $cm^{-2}\,s^{-1}\,sr^{-1}$, would produce a response equivalent to a second-order line of 500 erg $cm^{-2}\,s^{-1}\,sr^{-1}$. Thus we will take an estimate of the Fe XII contribution as $775 \pm 330$ erg $cm^{-2}\,s^{-1}\,sr^{-1}$, and use this to derive the density for the 186.88/195.12 ratio given in Table 20.

Within the error bars on the data, the density insensitive 364.47/195.12 ratio agrees with theory, although there is a suggestion that the second order 195.12 Å line is too weak relative to the first order 364.47 Å line. We compare this to Keenan et al. (1996) who have a theoretical value for the 364.47/195.12 ratio of 0.09, creating a far larger discrepancy with theory. This is due to the adoption by these authors of the Tayal & Henry (1988) collision strengths.

The 291.01/219.43 ratio also agrees within the error bars, but again there is a suggestion that the second order line is too weak.

With the revised estimate of the Fe XII 364.47 Å intensity mentioned above of 216 erg $cm^{-2}\,s^{-1}\,sr^{-1}$, we find excellent agreement between theory and observation for the 346.86/364.47 and 352.11/364.47 ratios in Table 19.

For the three density diagnostic ratios presented in Table 20 we find predicted densities of around $10^{10}$ $cm^{-3}$. The smallest error bars are found for the 338.27/364.47 ratio but, as noted above, there is a suggestion that the 338.27 Å may be blended.

### *13.5. Fe XIII*

There are 23 Fe XIII lines seen in the SERTS-89 spectrum—more than for any other ion—and there is a lot of density sensitivity due to the ground levels approaching Boltzmann equilibrium over the $10^8 - 10^{12}$ $cm^{-3}$ regime.

The line at 191.23 Å is identified as a blend of a S XI and a Fe XIII line, however the Fe XIII line expected at this wavelength is too weak to provide any appreciable intensity and so we dismiss this identification. As noted in Brickhouse et al. (1995) the unidentified line at 312.87 Å is in fact the Fe XIII $3s^23p^2\ ^3P_1 - 3s3p^3\ ^3P_0$ transition. Confirmation of this can be seen by the excellent agreement with theory of the density insensitive ratio 312.87/359.64 given in Table 19.

There are several discrepancies with the branching ratios given in Table 18, although the only major one is the 204.95/201.12 ratio. The problem here is probably with the second order 204.95 Å line being blended with a first order line at around 409.90 Å since previous first order observations of this line have always shown it to be significantly weaker than the

**Table 19.** Density insensitive ratios for the iron ions

| Ion | Ratio | Theory | SERTS-89 |
|---|---|---|---|
| Fe IX | 244.92 / 171.07 | $0.030 \pm 0.007$ | $0.11 \pm 0.05$ |
| Fe X | 345.74 / 174.53[b] | $0.053 \pm 0.010^{T}$ | $0.099 \pm 0.048$ |
| Fe XI | 341.11 / 352.67 | $0.29 \pm 0.04$ | $0.29 \pm 0.06$ |
| | 352.67 / 188.21 | $0.22 \pm 0.03^{T}$ | $0.11 \pm 0.03$ ◁ |
| Fe XII | 192.37[b]/ 195.12 | $0.25 \pm 0.03$ | $1.94 \pm 0.44$ |
| | 193.51 / 195.12 | $0.61 \pm 0.01$ | $1.05 \pm 0.26$ ◁ |
| | 219.43 / 196.62 | $0.73 \pm 0.04$ | $0.49 \pm 0.32$ |
| | 219.43 / 186.88[b] | $0.21 \pm 0.05$ | $0.10 \pm 0.05$ ◁ |
| | 291.01 / 219.44 | $0.41 \pm 0.06$ | $0.80 \pm 0.38$ |
| | 364.47 / 195.12 | $0.13 \pm 0.01^{T}$ | $0.18 \pm 0.04$ |
| | 346.86 / 364.47 | $0.35 \pm 0.01$ | $0.31 \pm 0.05$ |
| | 352.11 / 364.47 | $0.67 \pm 0.01$ | $0.67 \pm 0.11$ |
| | 283.45[i]/ 338.27 | $0.48 \pm 0.10$ | – |
| Fe XIII | 200.02[n]/ 203.82[s] | $0.20 \pm 0.02$ | – |
| | 204.25 / 203.82[s] | $0.14 \pm 0.02$ | $0.13 \pm 0.04$ |
| | 209.62 / 203.82[s] | $0.15 \pm 0.01$ | $0.09 \pm 0.05$ |
| | 201.12[b]/ [202,203]† | $0.14 \pm 0.02$ | $0.23 \pm 0.08$ |
| | 320.80 / 203.82[s] | $0.10 \pm 0.01^{T}$ | $0.16 \pm 0.03$ ◁ |
| | 348.18 / 202.04 | $0.12 \pm 0.01^{T}$ | $0.20 \pm 0.04$ ◁ |
| | 251.94 / [202,203]† | $0.22 \pm 0.02$ | $0.21 \pm 0.04$ |
| | 359.64 / 251.94 | $0.21 \pm 0.03$ | $0.40 \pm 0.08$ ◁ |
| | 312.17 / [348,359]‡ | $0.35 \pm 0.01$ | $0.31 \pm 0.05$ |
| | 312.87 / 359.64 | $0.38 \pm 0.01$ | $0.32 \pm 0.10$ |
| | 368.16[b]/ 320.80 | $0.74 \pm 0.05$ | $0.74 \pm 0.17$ |
| Fe XIV | 270.52 / 211.32 | $0.45 \pm 0.06$ | $0.48 \pm 0.09$ |
| | 274.21 / 211.32 | $0.35 \pm 0.03$ | $1.01 \pm 0.18$ ◁◁ |
| | 334.17 / 274.21 | $0.69 \pm 0.07$ | $0.62 \pm 0.10$ |
| | 444.24 / 334.17 | $0.015 \pm 0.002^{T}$ | $0.018 \pm 0.005$ |
| Fe XV | 417.25 / 284.16 | 0.031 | $0.045 \pm 0.007$ ◁ |
| | 327.03 / 284.16 | $0.011 \pm 0.001$ | $0.012 \pm 0.002$ |
| | 321.78 / 292.25[i] | $0.65 \pm 0.08$ | $0.81 \pm 0.30$ |
| | 243.78 / 284.16 | $0.056 \pm 0.005^{T}$ | $0.072 \pm 0.015$ |
| Fe XVI | 360.75 / 335.40 | 0.48 | $0.42 \pm 0.09$ |
| | 262.98 / 335.40 | $0.073 \pm 0.005^{T}$ | $0.063 \pm 0.013$ |
| | 251.07 / 262.98 | 0.60 | $0.68 \pm 0.14$ |
| Fe XVII | 350.48 / 254.89 | $0.41 \pm 0.04$ | $0.39 \pm 0.21$ |
| | 304.94[n]/ 350.48 | 0.18 | – |
| | 347.81 / 350.48 | $0.68 \pm 0.06^{T}$ | $0.68 \pm 0.24$ |
| | 358.25 / 350.48 | $0.30 \pm 0.01^{T}$ | $0.33 \pm 0.17$ |
| | 367.29 / 350.48 | $0.37 \pm 0.02$ | $0.36 \pm 0.20$ |
| | 389.08[b]/ 350.48 | $0.34 \pm 0.02^{T}$ | $0.61 \pm 0.18$ |
| | 409.71 / 350.48 | $0.57 \pm 0.02^{T}$ | $0.32 \pm 0.12$ ◁ |

† A blend of the 202.04 Å and 203.82 Å lines.
‡ A blend of the 348.18 Å and 359.64 Å lines.

201.12 Å line – see, e.g., the solar spectrum of Malinovsky & Heroux (1973).

The discrepancy in the 311.56/320.80 ratio is probably caused by a Cr XII line blending with the 311.56 Å line. The Cr XII transition is $3s^2 3p\ ^2P_{3/2} - 3s3p^2\ ^2P_{1/2}$ and by analogy with the corresponding transition in Fe XIV we can estimate its contribution to be around 5 erg cm$^{-2}$ s$^{-1}$ sr$^{-1}$, bringing the observed Fe XIII ratio into better agreement with theory.

The 240.72/251.94 branching ratio was noted to be inconsistent with the observations of Malinovsky & Heroux (1973) by Flower & Nussbaumer (1974) and we note that the same discrepancy is apparent in the SERTS-89 spectrum.

Although the observed 413.00/368.16 value matches its branching ratio within the error bars, 368.16 Å is identified as a blend with Cr XIII. Using the theoretical ratio in Table 17, we can estimate the Fe XIII component of this line as 105 erg cm$^{-2}$ s$^{-1}$ sr$^{-1}$, which then implies a Cr XIII contribution of 23 erg cm$^{-2}$ s$^{-1}$ sr$^{-1}$.

The density insensitive ratios given in Table 19 have been assessed over the density range $10^{8.5} - 10^{12.0}$ cm$^{-3}$. For the second order lines (those below 222 Å) we note that a line with intensity of around 200 erg cm$^{-2}$ s$^{-1}$ sr$^{-1}$ is predicted at 200.02 Å; however, this value falls below the $3\sigma$ sensitivity limit of 373 erg cm$^{-2}$ s$^{-1}$ sr$^{-1}$ for SERTS-89 at this wavelength. The Fe XIII component to the 201.12 Å blend can be estimated from the 201.12/(202.04,203.82) ratio given in Table 19 as around 240 erg cm$^{-2}$ s$^{-1}$ sr$^{-1}$; the other component is primarily Fe XII with an intensity as much as 154 erg cm$^{-2}$ s$^{-1}$ sr$^{-1}$ (see in Sect. 13.4).

For the lines found above 300 Å, the three ratios found in Table 19 show reasonable agreement with theory. In comparison with the second order lines, however, we find problems. The 320.80/203.82 and 348.18/202.04 ratios are both discrepant with theory, with the second order lines around 50% lower than theory predicts. This may seem like a simple first-order/second-order calibration problem, but we note that the first order line seen at 251.94 Å agrees with the second order lines but not the $>$ 300 Å lines as witnessed by the 251.94/(202.04,203.82) and 359.64/251.94 ratios. A detailed discussion of the SERTS-89 calibration is presented at the end of this paper.

After accounting for the redundancy provided by the density insensitive ratios, we are left with the three density sensitive ratios involving lines close in wavelength and the predicted densities are presented in Table 20. While 203.82/202.04 and 359.64/348.18 agree well with each other and are consistent with other ions formed at the same temperature, the 318.12/320.80 ratio gives a higher density. A possible explanation for this discrepancy stems from the fact that the 318.12 Å line is principally excited from the $^1D_2$ level in the ground configuration—the collision strengths from the $^3P$ levels are around 1 to 2 orders of magnitude weaker. However, at densities below $10^{10}$ cm$^{-3}$ the occupation numbers of the $^3P$ levels are around 1 to 2 orders of magnitude *higher* than the $^1D_2$ level, and so excitations from these levels will be contributing significantly to the intensity of the 318.12 Å line. To bring the 318.12/320.80 ratio in line with the other two, it is necessary that the collision strengths from the $^3P$ ground levels be *higher* than their current values.

### *13.6. Fe XIV*

Strong lines of Fe XIV are seen in the SERTS-89 spectrum, and they potentially yield excellent density diagnostics. The five branching ratios presented in Table 18 show good agreement with the observations apart from 257.40/270.52. As the observed ratio is less than the theoretical value, the obvious possibility is that the 270.52 Å line is blended with another line. The only candidate in the CHIANTI database is the Fe XXI 270.57 Å, which is not expected to be seen in the SERTS-89 spectrum. We note that if blending is a problem, the unknown component must have a considerable intensity, of the order of 250 erg cm$^{-2}$ s$^{-1}$ sr$^{-1}$.

Density insensitive ratios are presented in Table 19, and a major discrepancy can be seen in the 274.21/211.32 ratio. We do not expect the problem to be due to blending because the branching ratios for both lines agree well with the observations (Table 18). The 270.52/211.32 and 334.17/274.21 ratios both agree with theory, suggesting a distinction between those lines found above 274 Å and those found below 274 Å. This is further supported by the density sensitive ratios presented in Table 20; the 219.12/211.32 and 353.83/334.17 ratios both giving densities consistent with other ions formed at similar temperatures, while the 264.78/274.21 ratio suggests an extremely low density.

The resonance lines of Fe XIV have been observed in previous solar spectra and we look to see signs of an inconsistency in the 274.21/211.32 ratio. Malinovsky & Heroux (1973) give a value of $0.59 \pm 0.17$ (taking error bars of $\pm$ 20%); Behring et al. (1976) give $1.2 \pm 0.5$ (taking error bars of $\pm$ 30%); Keenan et al. (1991) give several sets of observations from the S082A instrument on Skylab with nine ratios of between 0.36 and 0.49 and another of 0.19. These latter observations seem more consistent with theory but, as noted by Bhatia et al. (1994), the S082A instrument response falls off rapidly below 220 Å and so we have to treat these values with caution. Overall, the data on the 274.21/211.32 ratio is confusing and seem to suggest that it varies with solar conditions. Observations with CDS may resolve these problems.

The discrepancy above and below 274 Å is more clearly demonstrated by the 274.21/270.52 ratio, since these are both strong lines and are close enough in wavelength so that calibration errors are minimized. As can be seen from Table 18, the CHIANTI value is $0.78 \pm 0.12$, whereas the SERTS-89 active region catalogue gives $2.11 \pm 0.37$. If 270.52 Å is actually a significant blend, as suggested above from branching ratio arguments, then the problem only gets much worse. Other unpublished SERTS observations using different optical components give ratios between 1.3 and 2.3 for quiet sun, off-limb, and various active regions. The Malinovsky & Heroux (1973) and Behring et al. (1976) values are $2.1 \pm 0.6$ and $1.6 \pm 0.7$, respectively. Blaha (1971) summarizes six early full-sun measurements that found ratios ranging from 1.3 to 1.7. The ten

Skylab values reported by Keenan et al. (1991) include those for three different active regions, yielding 1.2, 1.8, and 1.9. The remaining seven Skylab values are for various flares or flare sites, and show ratios between 0.73 and 0.95. While these latter observations may seem to match the CHIANTI prediction, Fe XXI 270.57 Å can become very important in flares, significantly reducing the expected 274.21/270.52 ratio. Thus, measurements of this ratio with many different instruments observing a wide variety of sources seem to be remarkably consistent, yet at serious variance with the best theoretical calculations presently available.

In addition to the above allowed transitions, three intercombination lines at 430–450 Å from $^2$P – $^4$P transitions are identified by Thomas & Neupert. However, the Fe XIV line predicted at 429.54 Å is several orders of magnitude weaker than the observed line and so we dismiss this identification. The remaining two lines are density sensitive and give a density in reasonable agreement with the two allowed ratios mentioned earlier, although we note the error bars on the data are considerably larger (Table 20).

Brickhouse et al. found the intensities of these $^2$P – $^4$P lines to be more than a factor of 3 too high compared to other Fe XIV lines. We get a similar result, but only when comparing them to lines below 274 Å, such as in the density insensitive ratio 444.24/211.32. In distinct contrast, we find the comparisons to lines above 274 Å are in good agreement with theory, as shown by the insensitive ratio 444.24/334.17 (Table 19). Clearly this is part of the same problem that has been discussed above, and we concur with Brickhouse et al. in suggesting that any problems with the $^2$P – $^4$P transitions merely indicate difficulties with the atomic physics for Fe XIV and do not reflect inaccuracies in the SERTS calibration.

Bhatia et al. (1994) presented new Distorted Wave calculations for Fe XIV, including for the first time the 3p$^3$ and 3s3p3d configurations, and presented comparisons with the SERTS-89 spectrum. The addition of the extra configurations has resulted in predictions of intensities for lines at 290.69 Å, 358.67 Å and 363.75 Å which are present in the SERTS-89 spectrum. We dispute that the 363.75 Å line can be ascribed primarily to Fe XIV as the Mg VII line at this wavelength accounts for most of the observed intensity (see Sect. 10.3), though Fe XIV may contribute a little. The 358.67 Å Fe XIV component may be important as the intensity at this wavelength in SERTS-89 can not be accounted for by Si XI, Ne IV and Fe XI lines alone (Sects. 8.3, 11.1, and 13.3). According to the Bhatia et al. (1994) calculations, these three Fe XIV lines are expected to have intensities of around 5–20 erg cm$^{-2}$ s$^{-1}$ sr$^{-1}$.

### *13.7. Fe XV*

The 417.25/284.16 ratio has long been acknowledged as discrepant with theory (see, e.g., Flower & Jordan 1971 and Feldman et al. 1992) and we find this the case in the SERTS-89 spectrum, although we note that Brickhouse et al. (1995) find marginal agreement with theory using the electron collision data from Pradhan (1988). The data in Table 19 show that we find the theoretical value to be around 25–50% below the observed value. The remaining insensitive ratios in Table 19 show good agreement with theory. Interestingly, it is the 327.03/284.16 ratio that agrees with theory rather than the 327.03/417.25 ratio.

**Table 20.** Density sensitive ratios for the iron ions

| Ion | Ratio | SERTS-89 | Log $N_e$ |
|---|---|---|---|
| Fe IX | 217.10 / 244.92 | $0.44 \pm 0.25$ | $8.3^{+1.5}_{-\mathrm{lo}}$ |
| | 244.92 / 241.75 | $0.83 \pm 0.39$ | $10.1^{+0.3}_{-1.4}$ |
| Fe X | 345.74 / 257.26[s] | $0.57 \pm 0.17$ | $9.0^{+0.7}_{-\mathrm{lo}}$ |
| Fe XI | 308.58 / 352.67 | $0.65 \pm 0.14$ | $11.2^{+\mathrm{hi}}_{-0.5}$ |
| | 349.04[b]/ 352.67 | $0.06 \pm 0.03$ | $9.2^{+0.3}_{-0.4}$ |
| Fe XII | 186.88[c]/ 195.12 | $0.64 \pm 0.29$ | $10.1^{+0.4}_{-0.6}$ |
| | 338.27 / 364.47 | $0.35 \pm 0.06$ | $10.3^{+0.2}_{-0.2}$ |
| | 219.43 / 195.12 | $0.11 \pm 0.05$ | $10.0^{+0.5}_{-0.7}$ |
| Fe XIII | 203.82[s]/ 202.04 | $1.64 \pm 0.37$ | $9.5^{+0.2}_{-0.2}$ |
| | 318.12 / 320.80 | $0.56 \pm 0.11$ | $10.2^{+0.2}_{-0.2}$ |
| | 359.64 / 348.18 | $1.15 \pm 0.19$ | $9.6^{+0.2}_{-0.2}$ |
| Fe XIV | 219.12 / 211.32 | $0.40 \pm 0.08$ | $9.5^{+0.1}_{-0.1}$ |
| | 264.78 / 274.21 | $1.01 \pm 0.17$ | $\leq 8.4$ |
| | 353.83 / 334.17 | $0.45 \pm 0.07$ | $9.7^{+0.1}_{-0.1}$ |
| | 447.34 / 444.24 | $2.9 \pm 0.7$ | $10.3^{+1.1}_{-0.5}$ |
| Fe XV | 321.78 / 327.03 | $0.41 \pm 0.11$ | $9.4^{+0.3}_{-0.4}$ |
| | 327.03 / 393.97 | $5.4 \pm 1.2$ | $\leq 8.8$ |

The Fe XV 312.55 Å line is blended with a Co XVII line. Given the Co XVII 339.54 Å line intensity, a comparison with the iso-electronic transitions of Fe XVI suggests that the Co XVII contribution to the 312.55 Å line is around 15 erg cm$^{-2}$ s$^{-1}$ sr$^{-1}$, leaving 51 erg cm$^{-2}$ s$^{-1}$ sr$^{-1}$ as due to Fe XV. Taking into account this contribution, the observed 312.55/327.03 value would then agree with the theoretical branching ratio shown in Table 18.

The Fe XV line at 372.76 Å is too weak to account for the whole of the observed line intensity—in the high density limit (i.e., above $10^{11}$ cm$^{-3}$), the 372.76/327.03 ratio is predicted to be 0.12, while the observed ratio of the lines is $0.19 \pm 0.05$. At the density predicted by the 321.78/327.03 ratio (Table 20) the 372.76/327.03 ratio falls to around 0.03–0.04.

The transitions identified at 292.392 Å and 304.874 Å originate from the same upper level (3p$^2$ $^3$P$_2$) and represent radiative decays down to the 3s3p $^3$P$_1$ and $^3$P$_2$ levels, respectively. The splitting of the these two levels is known from other lines in the Fe XV spectrum and so if we know the wavelength of one line we know the wavelength of the other. Doing this we find that if the 304.874 Å identification is correct (as would be expected since it is the stronger line) then it implies a line at 292.26 Å rather than 292.392 Å. There is in fact a line at 292.251 Å in the SERTS-89 spectrum (mistakenly identified as a Si X line, as shown in Sect. 9.4) and so we suggest that this line is actually the Fe XV 3s3p $^3$P$_1$ – 3p$^2$ $^3$P$_2$ transition.

With this identification, we can then estimate the contribution of Fe XV to the blend at 304.87 Å as being around 120

erg $cm^{-2}$ $s^{-1}$ $sr^{-1}$. The other two components to this blend are from Fe XVII (not identified) and Mn XIV. The Fe XVII component is negligible and can be estimated to be 4 erg $cm^{-2}$ $s^{-1}$ $sr^{-1}$ (see Sect. 13.9), while the Mn XIV component can be estimated at around 50–60 erg $cm^{-2}$ $s^{-1}$ $sr^{-1}$ by comparison with Mn XV 360.96 Å and the iso-electronic transitions in Fe XV and Fe XVI. The combined total is then in good agreement with the observed blend intensity of 206 erg $cm^{-2}$ $s^{-1}$ $sr^{-1}$.

Keenan et al. (1993b) suggest the identification of a line at 324.97 Å from Skylab spectra, which is not identified in the SERTS-89 spectrum. However we note that this line is density insensitive relative to the 327.03 Å line, with a value of $0.025 \pm 0.004$, while the corresponding 324.97/327.03 ratio in the Skylab spectra presented in Keenan et al. has an average value of 0.09, casting doubts on the identification of this line.

Of the ten Fe XV lines identified in SERTS-89, we can dismiss three lines as being mis-identifications (256.91 Å, 292.39 Å, and 372.76 Å), and add one that had incorrectly been called Si X (292.25 Å). In addition, Brickhouse et al. have already noted that the unidentified line at 393.97 Å is probably the forbidden Fe XV $3s3p\ ^3P_2 - 3s^2\ ^1S_0$ transition, an identification that we also adopt. We can form three groups of insensitive lines. Group 1 (243.78 Å, 284.16 Å, 312.55 Å, 327.03 Å and 417.25 Å) shows internal consistency apart from the well-documented case of 417.25 Å, while Group 2 (292.25 Å, 304.87 Å and 321.78 Å) shows reasonable agreement. Group 3 consists of just the 393.97 Å line.

Taking any ratio between lines of the different groups yields a density diagnostic, and we choose 321.78/327.03 and 327.03/393.97 with results shown in Table 20. The low density derived from the 327.03/393.97 ratio suggests the 393.97 Å line is possibly blended.

### *13.8. Fe XVI*

There are five transitions between the n=3 configurations of Fe XVI and they all appear in the SERTS-89 spectrum. All the ratios are density insensitive, although there is some temperature sensitivity in the 3s–3p/3p–3d ratios. Comparisons with observations are given in Table 18 and Table 19. Surprisingly the only major discrepancy is for the single branching ratio 265.02/251.07. By virtue of the excellent agreement for the density insensitive ratio involving the 251.07 Å line given in Table 19, we surmise that it is the 265.02 Å line causing the problem, in which case the observed intensity of the latter line is lower than theory predicts and so blending can not be invoked. We note that Skylab measurements of this ratio presented by Keenan et al. (1994c) range between 0.13 and 0.23, more consistent with theory and so we suggest there may be a problem with the reported SERTS-89 observation of the 265.02 Å line. In fact, an improved fit to this line in the SERTS-89 data is given in Table 24, and it provides a 265.02/251.07 ratio of $0.19 \pm 0.06$, which is now in excellent agreement with the predicted value.

### *13.9. Fe XVII*

There are many weak 3s–3p and 3p–3d transitions expected in the 200–320 Å region, but only the 254.89 Å line is strong enough to be observed by SERTS-89. Above 320 Å, the higher sensitivity of the instrument allows several 3s–3p transitions to be clearly identified.

In addition to the lines in the SERTS catalogue, Brickhouse et al. (1995) identify the feature observed at 367.287 Å as an Fe XVII line. We confirm this and give the transition information in Table 23. The intensity of the line is in excellent agreement with theory, as witnessed by the data in Table 19.

Taking ratios relative to the 350.48 Å line, all the lines agree well with theory except for 409.71 Å, which is around a factor of 2 too low. The reasons for this are unclear. The 389.08 Å line is blended with an Ar XVI line, and we estimate an Fe XVII contribution of around 7.1 erg $cm^{-2}$ $s^{-1}$ $sr^{-1}$ to the total of 12.8 erg $cm^{-2}$ $s^{-1}$ $sr^{-1}$, which is consistent with the estimate made for the Ar XVI line in Sect. 7.2. A line is predicted by CHIANTI at 304.94 Å, making it a potential blend with the observed 304.87 Å line identified as Mn XIV plus Fe XV. However, the density insensitive 304.94/350.48 ratio shows that the expected Fe XVII intensity of this line is only around 4 erg $cm^{-2}$ $s^{-1}$ $sr^{-1}$, less than 2% of the other components.

Although good agreement with theory has been found for Fe XVII, we note that four of the transition identifications of CHIANTI disagree with those of Thomas & Neupert. In particular, the 254.892 Å line is given by CHIANTI as a $^3P_1$–$^1S_0$ transition, 347.814 Å as a $^3P_1$–$^1D_2$ transition, 358.247 Å as a $^1P_1$–$^3P_1$ transition, and 389.075 Å as a $^1P_1$–$^3D_2$ transition. The reason for these discrepancies stem from the use in CHIANTI of atomic data from Bhatia & Doschek (1992), who adopted different term designations than those used in previous work – see, e.g., Jupén (1984).

## 14. The nickel ions

Lines from nickel ions Ni XIV–XVIII are seen in the SERTS-89 spectrum, although the CHIANTI database presently includes only Ni XV and Ni XVIII. As a general rule, the nickel ion lines show similar behaviour to their iron counterparts, apart from density sensitivity where the nickel line ratios are sensitive to slightly higher density ranges.

### *14.1. Ni XIV*

Two lines are identified in the SERTS-89 spectrum, and we note that they are the iso-electronic analogues to Fe XII 352.11 Å and 364.47 Å which form a density insensitive pair (see Sect. 13.4). If we assume that the atomic data for Ni XIV will be approximately the same as for Fe XII, then we would expect the Ni XIV ratio to also be density insensitive with a value similar to the Fe XII ratio. We thus give the Ni XIV ratio in Table 21, with the theoretical value simply being that of Fe XII. As can be seen, the observed value strongly disagrees with the theoretical value, and indicating that some other ion must be responsible for most of the intensity seen at 302.29 Å.

**Table 21.** Insensitive ratios for the nickel ions.

| Ion | Ratio | Theory | SERTS-89 |
|---|---|---|---|
| Ni XIV | 302.29 / 316.60 | $0.67 \pm 0.01$ | $7.8 \pm 4.1$ ◁◁ |
| Ni XVIII | 236.34 / 291.99 | $0.0059 \pm 0.0010^{\mathrm{T}}$ | $0.69 \pm 0.31$ ◁◁ |
| | 320.56 / 291.99 | 0.48 | $0.43 \pm 0.07$ |

**Table 22.** Density sensitive ratios for the nickel ions

| Ion | Ratio | SERTS-89 | Log $N_{\mathrm{e}}$ |
|---|---|---|---|
| Ni XV | 311.79[c]/ 298.12 | $0.75 \pm 0.45$ | $9.9^{+0.3}_{-0.5}$ |

### *14.2. Ni XV*

Three lines are identified in the spectrum and two are blended. From the analysis of the Mg VIII lines in Sect. 9.2, we can estimate a Ni XV contribution of 31 erg cm$^{-2}$ s$^{-1}$ sr$^{-1}$ to the 311.79 Å line. The 311.79/298.12 ratio is strongly density sensitive, providing a density value of $10^{9.9}$ cm$^{-3}$.

The contribution of Ni XV to the blend at 319.02 Å is difficult to estimate as the Ni XV line is density sensitive relative to both the 298.12 Å and 311.79 Å lines. The 319.02/311.79 ratio is least sensitive and at the predicted density of $10^{9.9}$ cm$^{-3}$ it takes the value 0.8, allowing us to deduce contributions of 25 erg cm$^{-2}$ s$^{-1}$ sr$^{-1}$ and 51 erg cm$^{-2}$ s$^{-1}$ sr$^{-1}$ to the 319.02 Å line from Ni XV and Mg VII respectively. The Mg VII value is used in Sect. 10.3.

The three lines seen are analogous to the 348.18 Å, 359.64 Å and 368.16 Å lines of Fe XIII.

### *14.3. Ni XVIII*

Three lines are identified for Ni XVIII and they are all density insensitive relative to each other. We give comparisons with theory in Table 21. A large discrepancy can be seen for the 236.34/291.99 ratio suggesting another ion must be responsible for the 236.34 Å line.

## 15. Summary and discussion

### *15.1. Calibration of SERTS-89*

The large number of lines and high signal-to-noise of the SERTS-89 spectrum mean that we can bring together the many density insensitive ratios identified over the previous sections and try to answer the questions raised in several places about the instrument calibration. The main concern has been with the intensities of the lines found above 400 Å and we proceed to analyse this as follows.

For two lines at wavelengths $\lambda_1$ and $\lambda_2$ with observed intensities $I(\lambda_1)$ and $I(\lambda_2)$, we denote the observed ratio of the two lines as $O_{12} = I(\lambda_1)/I(\lambda_2)$, while we give the CHIANTI ratio as $T_{12}$.

In Fig. 1 we plot the values of $O_{12}/T_{12}$ for all density insensitive line pairs given in the previous sections except those for which we have identified problems due to blending or atomic physics inaccuracies. For each ratio, we calculate a weighting $W$ such that, if $O_{12}/T_{12} = R \pm E$, then $W = 2E/R$. Graphically, different weightings are represented by the symbols:

| | |
|---|---|
| $W > 0.75$ | ○ |
| $0.75 \geq W > 0.53$ | □ |
| $0.53 \geq W > 0.42$ | ● |
| $0.42 \geq W$ | black square |

The partitioning of $W$ is chosen to provide equal numbers of ratios in each group.

In Fig. 2 we display the same observations/theory comparison but with a new calibration scale used. This new scale is specified by the function $\eta(\lambda)$, which is such that if, on the original scale, a particular observed ratio was $I(\lambda_1)/I(\lambda_2)$ then on the new scale the value will be

$$\frac{I(\lambda_1)}{I(\lambda_2)} \times \frac{\eta(\lambda_2)}{\eta(\lambda_1)}.$$

Accordingly the original value of $O_{12}/T_{12}$ is mapped to

$$\frac{O_{12}}{T_{12}} \times \frac{\eta(\lambda_2)}{\eta(\lambda_1)}.$$

The particular $\eta$ function used to generate Fig. 2 is shown in Fig. 3, and has been chosen to increase the intensities of the lines found above 400 Å by a factor of up to 2.

The suggestion in the Ne VI, Mg VIII and Mg VII sections that the SERTS-89 calibration may need revision over the 430–450 Å region is demonstrated by a comparison of Figs. 1 and 2: the filled-in symbols – corresponding to smaller error bars – clearly fall into better alignment in Fig. 2. The major exceptions to this are the Fe XIV 444.24/334.17 and C IV 419.72/384.17 ratios. A similar calibration adjustment was considered by Bhatia & Thomas (1997) based on their analysis of Mg VIII. They point out, however, that C IV and Mg IX ratios presented by Keenan et al. (1993a,1994a) seem to confirm the published SERTS relative calibration, whereas Fe XIV lines studied by Brickhouse et al. (1995) imply that it may actually be too low at the long wavelength end (thus requiring $\eta > 1$). We have discussed the latter work in Sect. 13.6, and feel that it merely reflects errors in the Fe XIV atomic data; while for Mg IX we have used different atomic data to Keenan et al. (1994a) and find that it now produces the same discrepancy as the other Mg and Ne ions. Overall we feel that the insensitive ratios looked at here strongly hint at a problem with the SERTS-89 calibration above around 430 Å, but definitive resolution of this issue will only be possible with further observations of this wavelength region.

Brickhouse et al. (1995) have also claimed that second order lines appear to be lower in intensity with regard to first order lines by around 50% in the SERTS-89 catalogue. Our study confirms that some second order lines of Fe IX, Fe X, Fe XII, Fe XIII and Fe XIV do indeed show evidence of being too weak relative to first order lines. However, we note the following: the Fe XI 352.67/188.21 ratio implies that the second order 188.21 Å line

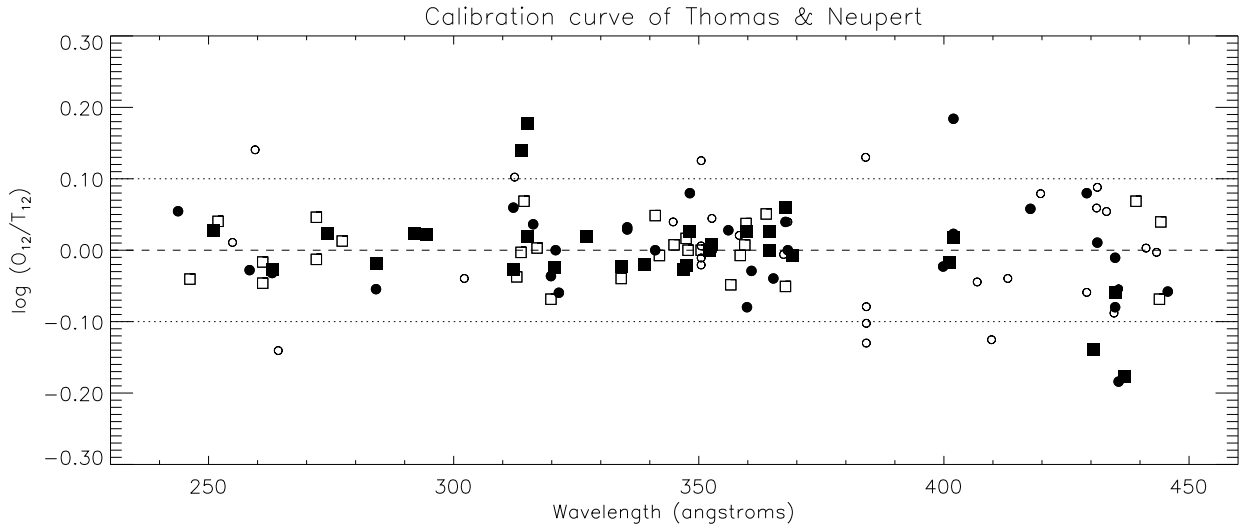


**Fig. 1.** Comparison of observations with theory for density insensitive ratios, using line intensities published by Thomas & Neupert. The shaded symbols indicate ratios with smaller error bars – see the text for more details.

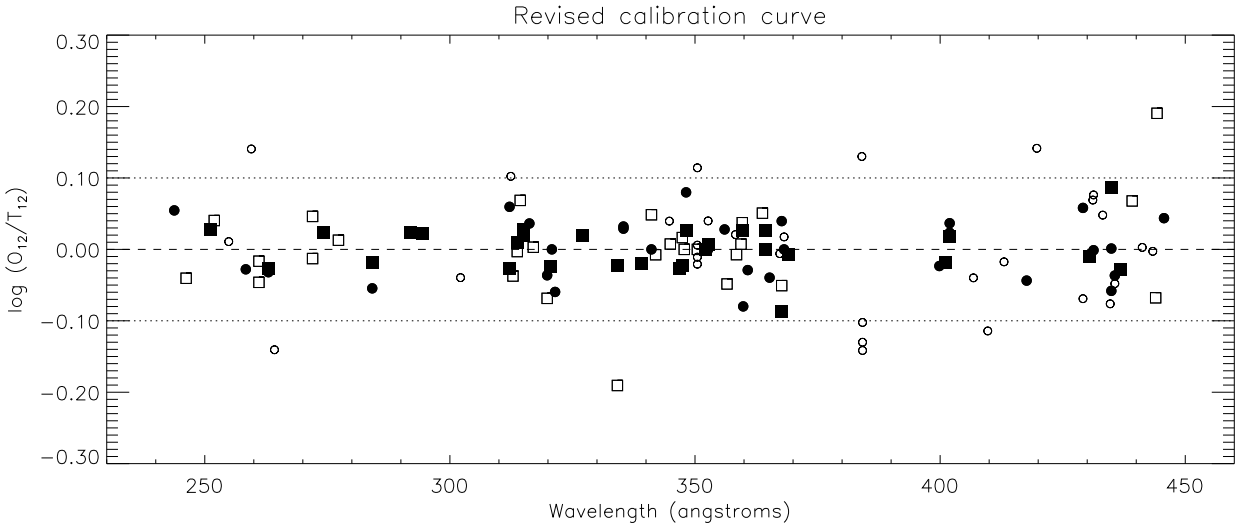


**Fig. 2.** Same comparison as above but with line intensities adjusted by a factor $\eta(\lambda)$.

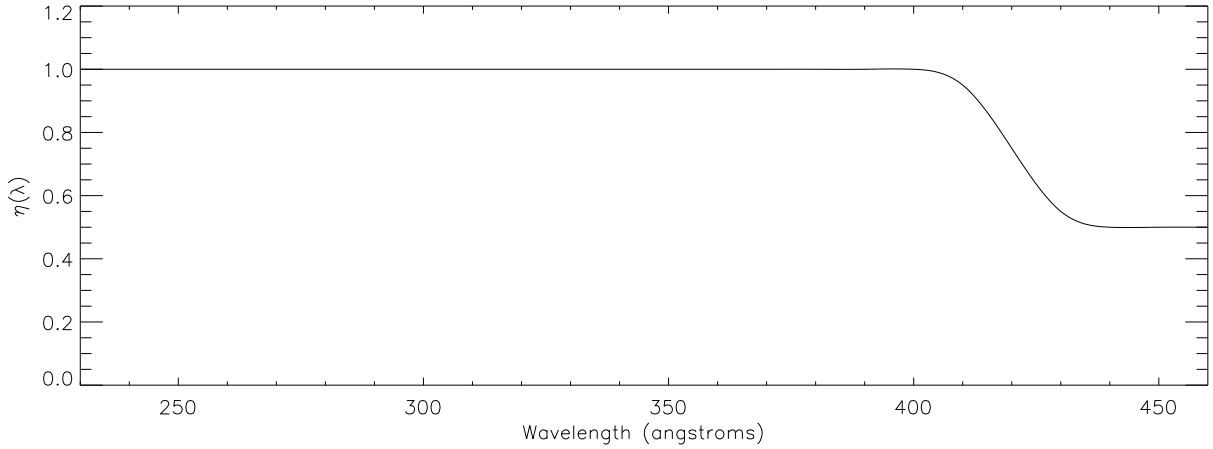


**Fig. 3.** Plot of the function $\eta(\lambda)$ used to derive Fig. 2 (not on the same vertical scale).

**Table 23.** New identifications for reported lines in the SERTS-89 catalogue. A 'b' indicates that the identified transition is a blended component of a line already listed in the spectrum, 'm' that the line had been mistakenly attributed to some other ion. Identifications first suggested by Brickhouse et al. (1995) are marked with 'B', that by Dwivedi et al. (1997) with 'D', and that by Keenan et al. (1996) with 'K'.

| Wavelength (Å) | Ion | Transition |
|---|---|---|
| 276.850[b] | Si VII | $2s^2 2p^4\ ^3P_0 - 2s2p^5\ ^3P_1$ |
| 278.407[b] | Si VII | $2s^2 2p^4\ ^3P_1 - 2s2p^5\ ^3P_2$ |
| 283.486[K] | N IV | $2s2p\ ^3P_{0,1,2} - 2s3d\ ^3D_{1,2,3}$ |
| 292.251[m] | Fe XV | $3s3p\ ^3P_1 - 3p^2\ ^3P_2$ |
| 311.555[b] | Cr XII | $3s^2 3p\ ^2P_{3/2} - 3s3p^2\ ^2P_{1/2}$ |
| 312.868[B] | Fe XIII | $3s^2 3p^2\ ^3P_1 - 3s3p^3\ ^3P_0$ |
| 314.592[D] | Mg VI | $2s^2 2p^3\ ^2P_{3/2}$ - $2s2p^4\ ^2S_{1/2}$ |
| 357.954[b] | Ne V | $2s^2 2p^2\ ^3P_0 - 2s2p^3\ ^3S_1$ |
| 358.667[b] | Ne IV | $2s^2 2p^3\ ^2D_{5/2} - 2s2p^4\ ^2P_{1/2}$ |
| " | Si XI | $2s2p\ ^3P_1 - 2p^2\ ^3P_2$ |
| " | Fe XIV | $3s3p^2\ ^2D_{5/2} - 3p^3\ ^2D_{5/2}$ |
| 364.468[b] | Si XI | $2s2p\ ^3P_1 - 2p^2\ ^3P_1$ |
| 365.565[b] | Ne V | $2s^2 2p^2\ ^1D_2 - 2s2p^3\ ^1P_1$ |
| 367.287[B] | Fe XVII | $2s^2 2p^5 3s\ ^3P_2 - 2s^2 2p^5 3p\ ^3D_2$ |
| 373.766[b] | O III | $2s^2 2p^2\ ^3P_1 - 2s^2 2p3s\ ^3P_2$ |
| 374.160[b] | N III | $2s^2 2p\ ^2P_{1/2} - 2s^2 3d\ ^2D_{3/2}$ |
| 393.969[B] | Fe XV | $3s^2\ ^1S_0 - 3s3p\ ^3P_2$ |
| 406.791[B] | Fe XI | $3s^2 3p^4\ ^1D_2 - 3s3p^5\ ^3P_2$ |

is too strong relative to the first order 352.67 Å line by a factor of around 2; for Fe IX the problem with the 171.07 Å line has been seen in many previous spectra; in Sect. 13.5 we noted that while the second order Fe XIII lines are too low relative to the first order lines above 300 Å, they are consistent with the first order line seen at 251.94 Å; there are many difficulties with the Fe XIV lines and while a stronger 211.32 Å intensity would alleviate some of these difficulties (e.g., the 274.20/211.32 ratio) it would not affect others (e.g., the 270.52/274.20 ratio). We also note that most of the second order lines are 3p–3d transitions in the iron ions, and the density insensitive ratios involve comparisons with 3s–3p transitions. Thus another possibility is that the observations may simply reflect atomic physics inaccuracies in comparing these two types of transition. Therefore, we do not feel that any significant modification of the SERTS-89 second-order calibration is called for on the basis of our present analysis.

### *15.2. Revisions to the SERTS-89 catalogue*

The revisions to the SERTS-89 catalogue suggested by the previous analysis are displayed in Tables 23, 24 and 25. Table 23 gives identifications both for lines reported as unidentified in the catalogue and for newly-identified components to blended lines. Table 24 contains new spectral line fits obtained since original publication of the spectrum, and Table 25 gives lines which have been mis-identified in Thomas & Neupert but for which there are no other viable candidates in the CHIANTI database.

**Table 25.** Lines for which the theoretical estimate of the line intensity is far less than the observed value, indicating an incorrect identification but with no other CHIANTI candidates. Those marked with 'D' have also been noted as erroneous by Dwivedi et al. (1997).

| Wavelength (Å) | Prior Identification |
|---|---|
| 200.408 (400.816) | Fe XII |
| 204.251 (408.502) | Fe XIII |
| 215.288 (430.576) | O V |
| 236.335 | Ni XVIII |
| 292.392 | Fe XV |
| 302.288 | Ni XIV |
| 319.726[D] | Mg VI |
| 338.375[D] | Si VIII |
| 372.758 | Fe XV |
| 376.625[D] | Mg V |
| 427.843 | Ne III |
| 429.540 | Fe XIV |

### *15.3. Conclusions*

Although much of this paper has been spent discussing discrepancies between theory and observation, in fact such cases are relatively few considering the vast amount of detailed, quantitative information that is now available in both the CHIANTI database and the published SERTS-89 spectrum. For the great majority of lines there is good to excellent agreement between the SERTS-89 measurements and CHIANTI predictions. One important new result is the ability to quantify the effects of unavoidable blends, and thus make a number of additional spectral lines available for spectroscopic analyses. Several new useful lines, suggested by theory, have subsequently been found and measured in the data. Numerous new line identifications have been made, and many others have been tested and confirmed (or sometimes rejected). We have shown that the technique of selecting lines for spectroscopic diagnostics only after validation of branching/insensitive ratios leads to a substantial reduction in the scatter of derived densities, producing much more definitive measurements of solar plasma parameters. Where discrepancies do exist, they point out potential mis-identifications, additional blending, possible calibration problems, data reduction errors, or areas where theoretical calculations need to be improved. Some of these are correctable, even further strengthening the value of both CHIANTI and SERTS data sets. And in those cases, the confrontation of theory against measurements often provides the direct clues that lead to the eventual solution of the problem. While some inevitable limitations remain, and future improvements are suggested in several areas, the excellent overall consistency between theory and observation demonstrated in this paper provides considerable confidence in the present accuracy of the atomic data in the CHIANTI database, and in the high quality of the SERTS-89 spectral measurements.

The identification of the many density insensitive line ratios given here and their verification through the SERTS-89 spectrum will be useful for future EUV missions as a means

**Table 24.** New spectral line fits not in the original SERTS-89 catalogue. Those marked 'r' replace the previously published fit, 'K' are from Keenan et al. (1996), 'D' are from Dwivedi et al. (1997). The feature at 283.700Å is discussed in Sect. 13.4. Intensities are given on the old absolute calibration scale.

| Wavelength (Å) | Intensity (erg cm$^2$ s$^{-1}$ sr$^{-1}$) | FWHM (Å) | Ion | Transition |
|---|---|---|---|---|
| $196.618 \pm 0.003^{K}$ | $279 \pm 139$ | $0.048 \pm 0.011$ | Fe XII | $3p^3\ ^2D_{5/2} - 3p^23d\ ^2D_{5/2}$ |
| $216.936 \pm 0.004^{D}$ | $30.6 \pm 23.5$ | $0.028 \pm 0.013$ | Si VIII | $2s^22p^3\ ^2D_{5/2} - 2s2p^4\ ^2P_{3/2}$ |
| $247.159 \pm 0.009$ | $85 \pm 41$ | $0.082 \pm 0.023$ | S XI | $2s^22p^2\ ^3P_2 - 2s2p^3\ ^3P_1$ |
| $257.144 \pm 0.006^{D}$ | $28.8 \pm 17.8$ | $0.036 \pm 0.016$ | S X | $2s^22p^3\ ^4S_{3/2} - 2s2p^4\ ^4P_{1/2}$ |
| $265.003 \pm 0.006^{r}$ | $84 \pm 25$ | $0.093 \pm 0.016$ | Fe XVI | $3p\ ^2P_{3/2} - 3d\ ^2D_{3/2}$ |
| $272.555 \pm 0.003^{D}$ | $19.8 \pm 9.8$ | $0.045 \pm 0.008$ | Si VII | $2s^22p^4\ ^3P_2 - 2s2p^5\ ^3P_1$ |
| $275.617 \pm 0.012^{D}$ | $17.6 \pm 13.8$ | $0.060 \pm 0.031$ | Si VII | $2s^22p^4\ ^3P_1 - 2s2p^5\ ^3P_1$ |
| $276.148 \pm 0.002^{D}$ | $21.9 \pm 9.2$ | $0.047 \pm 0.006$ | Mg VII | $2s^22p^2\ ^3P_0 - 2s2p^3\ ^3S_1$ |
| $276.600 \pm 0.003^{D}$ | $22.4 \pm 12.3$ | $0.067 \pm 0.010$ | Mg V | $2s^22p^4\ ^1D_2 - 2s2p^5\ ^1P_1$ |
| $280.749 \pm 0.003^{D}$ | $9.4 \pm 7.5$ | $0.045 \pm 0.010$ | Mg VII | $2s^22p^2\ ^1D_2 - 2s2p^3\ ^1P_1$ |
| $283.700 \pm 0.007^{K}$ | $18.2 \pm 9.2$ | $0.061 \pm 0.016$ | | |
| $291.359 \pm 0.006^{D}$ | $10.3 \pm 6.3$ | $0.037 \pm 0.015$ | Mg VI | $2s^22p^3\ ^2P_{1/2,3/2} - 2s2p^4\ ^2P_{1/2}$ |
| $293.146 \pm 0.006^{D}$ | $14.0 \pm 8.1$ | $0.037 \pm 0.015$ | Mg VI | $2s^22p^3\ ^2P_{1/2,3/2} - 2s2p^4\ ^2P_{3/2}$ |
| $296.128 \pm 0.009^{r}$ | $146 \pm 31$ | $0.093 \pm 0.015$ | Si IX | $2s^22p^2\ ^3P_2 - 2s2p^3\ ^3P_2$ |
| $296.228 \pm 0.032^{r}$ | $34 \pm 26$ | $0.080 \pm 0.054$ | Si IX | $2s^22p^2\ ^3P_2 - 2s2p^3\ ^3P_1$ |
| $352.213 \pm 0.009^{D}$ | $4.3 \pm 3.1$ | $0.045 \pm 0.021$ | Mg V | $2s^22p^4\ ^3P_1 - 2s2p^5\ ^3P_0$ |
| $387.769 \pm 0.006^{D}$ | $3.8 \pm 1.5$ | $0.061 \pm 0.016$ | Mg VI | $2s^22p^3\ ^2P_{1/2} - 2s2p^4\ ^2D_{3/2}$ |
| $387.966 \pm 0.009^{r}$ | $6.2 \pm 2.3$ | $0.104 \pm 0.025$ | Mg VI | $2s^22p^3\ ^2P_{3/2} - 2s2p^4\ ^2D_{5/2}$ |
| $388.228 \pm 0.002^{D}$ | $1.4 \pm 0.8$ | $0.042 \pm 0.007$ | Ne IV | $2s^22p^3\ ^2P_{1/2,3/2} - 2s2p^4\ ^2P_{3/2}$ |
| $434.691 \pm 0.006$ | $2.3 \pm 1.3$ | $0.064 \pm 0.015$ | Mg VII | $2s^22p^2\ ^3P_2 - 2s2p^3\ ^3D_2$ |

of checking the calibration of the instruments. In a reciprocal manner these future missions may also reveal more information about the problems discussed here. As an example, the Coronal Diagnostic Spectrometer (CDS) on the recently launched Solar and Heliospheric Observatory contains two EUV spectrometers – the grazing incidence (GIS) and the normal incidence (NIS); both described in more detail in Harrison et al. (1995). Although neither spectrometer has better spectral resolution than SERTS, they both have the ability to observe the same lines in a huge range of different conditions, giving information on the composition of blends and checking the range of density sensitivity of line ratios. For both instruments, the use of density insensitive line ratios is underway in attempt to assess the quality of the laboratory calibration – a preliminary investigation of the NIS calibration can be found in Landi et al. (1997).

In this paper we have have been primarily interested in comparing the CHIANTI atomic data with the SERTS-89 spectrum and as a by-product have predicted electron densities for a number of different ions. A future paper will utilize this information to infer information about the solar atmosphere.

*Acknowledgements.* PRY acknowledges the financial support of PPARC. RJT acknowledges support of the SERTS sounding rocket program through grants from the Solar Physics Office of NASA's Space Physics Division.

## References

Arnaud M., Raymond J. C., 1992, ApJ 398, 394
Arnaud M., Rothenflug R., 1985, A&AS 60, 425
Behring W. E., Cohen L., Feldman U., Doschek G. A., 1976, ApJ 203, 521
Bely O., Faucher P., 1970, A&A 6, 88
Berrington K. A., 1985, J. Phys. B 18, L395
Bhatia A. K., Doschek G. A., 1992, ADNDT 52, 1
Bhatia A. K., Doschek G. A., 1995, ADNDT 60, 97
Bhatia A. K., Thomas R. J., 1997, ApJ *submitted*
Bhatia A. K., Kastner S. O., Keenan F. P., Conlon E. S., Widing K. G., 1994, ApJ 427, 497
Blaha M., 1971, Sol. Phys. 17, 99
Brickhouse N. S., Raymond, J. C., Smith, B. W., 1995, ApJS 97, 551
Dere K. P., Landi E., Mason H. E., Monsignori-Fossi B. F., Young P. R., 1997, A&AS *in press*
Dwivedi B. N., Mohan A., Thomas R. J., 1997, Sol. Phys. *submitted*
Fawcett B. C., Mason H. E., 1991, ADNDT 47, 17
Feldman U., 1992, ApJ 385, 758
Feldman U., Laming J. M., Mandelbaum P., Goldstein W. H., Osterheld A., 1992, ApJ 398, 692
Flower D. R., 1977, A&A 54, 163
Flower D. R., Jordan C., 1971, A&A 14, 473
Flower D. R., Nussbaumer H., 1974, A&A 31, 353
Foster V. J., Keenan F. P., Reid R. H. G., 1997, ADNDT *in press*
Harrison R. A., Sawyer E. C., Carter M. K., et al., 1995, Sol. Phys. 162, 233.
Heil T. G., Kirby K., Dalgarno A., 1983, Phys. Rev. A 27, 2826
Hummer D. G., Berrington K. A., Eissner W., et al., 1993, A&A 279, 298
Jupén C., 1984, MNRAS 208, 1P
Jupén C., Isler R. C., Trabërt, E., 1993, MNRAS 264, 627

Keenan F. P., 1988, Phys. Scripta 37, 57
Keenan F. P., Dufton P. L., Boylan M. B., Kingston A. E., Widing K. G., 1991, ApJ 373, 695
Keenan F. P., Thomas R. J., Neupert W. M., Conlon E. S., V. M. Burke, 1993a, Sol. Phys. 144, 69
Keenan F. P., Dufton P. L., Conlon E. S., et al., 1993b, ApJ 405, 798
Keenan F. P., Thomas R. J., Neupert W. M., Conlon E. S., 1994a, Sol. Phys. 149, 301
Keenan F. P., Conlon E. S., Bowden D. A., Dwivedi B. N., Widing K. G., 1994b, Sol. Phys. 149, 137
Keenan F. P., Conlon E. S., Foster V. J., Tayal S. S., Widing K. G., 1994c, ApJ 432, 809
Keenan F. P., Thomas R. J., Neupert W. M., et al., 1996, MNRAS 278, 773
Laming J. M., Drake J. J., Widing K. G., 1995, ApJ 443, 416
Landi E., Landini M., 1997, A&A *in press*
Landi E., Landini M., Pike C. D., Mason H. E., 1997, Sol. Phys. *in press*
Landman D. A., 1975, A&A 43, 285
Malinovsky M., Heroux L., 1973, ApJ 181, 1009
Neupert W. M., Kastner S. O., 1983, A&A 128, 181
Pradhan A. K., 1988, ADNDT 40, 355
Tayal S. S., Henry R. J. W., 1988, ApJ 329, 1023
Thomas R. J., Neupert W. M., 1994, ApJS 91, 461
Young P. R., Mason H. E., 1996, EUV Density Diagnostics in Solar and Stellar Spectra. In: Pallavicini R., Dupree A. K. (eds.) Proc. of the 9th Cool Stars Workshop, Cool Stars, Stellar Systems, and the Sun. A. S. P. Conf. Ser. Vol. 109, p. 301
Zhang H. L., Sampson D. H., 1992, ADNDT 52, 143

This article was processed by the author using Springer-Verlag LaTeX A&A style file *L-AA* version 3.